BRNO UNIVERSITY OF TECHNOLOGY
VYSOKÉ UČENÍ TECHNICKÉ V BRNĚ

FACULTY OF MECHANICAL ENGINEERING
FAKULTA STROJNÍHO INŽENÝRSTVÍ

INSTITUTE OF AEROSPACE ENGINEERING
LETECKÝ ÚSTAV

SIMULATION OF ULTRASONIC WAVE IN THE COMPOSITE AIRCRAFT STRUCTURES

SIMULACE ŠÍŘENÍ ULTRAZVUKOVÝCH VLN V CELOKOMPOZITNÍCH TENKOSTĚNNÝCH KONSTRUKCÍCH

MASTER'S THESIS
DIPLOMOVÁ PRÁCE

AUTHOR — Bc. Jan Cimrhanzl
AUTOR PRÁCE

SUPERVISOR — Ing. Jan Šplíchal, Ph.D.
VEDOUCÍ PRÁCE

BRNO 2016

VYSOKÉ UČENÍ TECHNICKÉ V BRNĚ
FAKULTA STROJNÍHO INŽENÝRSTVÍ

Zadání diplomové práce

Ústav:	Letecký ústav
Student:	**Bc. Jan Cimrhanzl**
Studijní program:	Strojní inženýrství
Studijní obor:	Stavba letadel
Vedoucí práce:	**Ing. Jan Šplíchal, Ph.D.**
Akademický rok:	2015/16

Ředitel ústavu Vám v souladu se zákonem č.111/1998 o vysokých školách a se Studijním a zkušebním řádem VUT v Brně určuje následující téma diplomové práce:

Simulace šíření ultrazvukových vln v celokompozitních tenkostěnných konstrukcích

Stručná charakteristika problematiky úkolu:

Popište současný stav v problematice simulací šíření ultrazvukových vln v tenkostěnných celokompozitních konstrukcích metodou konečných prvků (MKP) a metod Structural Health Monitoring (SHM). Na základě zjištěných informací vytvořte MKP model a ověřte možnosti modelování šíření ultrazvukových vln a detekce poškození v celokompozitních tenkostěnných konstrukcích. Jako základní konstrukci zvolte kompozitní potahový panel dle definice vedoucího diplomové práce.
Pro tyto MKP modely využijte systém MSC.Patran/MSC.Nastran a MSC.Patran/MSC.Dytran.

Cíle diplomové práce:

1.Popis současného stavu metod SHM a mkp simulací v oblasti šíření ultrazvukových vln
2Vytvoření MKP modelu desky pro simulaci šíření ultrazvukových vln v MSC.Patran/MSC.Nastran
3.Vytvoření MKP modelu desky pro simulaci šíření ultrazvukových vln v MSC.Patran/ MSC.Dytran
4. Porovnejte oba řešiče

Seznam literatury:

Ahmed N. M. (2014): A Study of Guided Ultrasonic Wave Propagation Characteristics in Thin Aluminium Plate for Damage Detection Master Science Defree in Civil Engineering, The University of Toledo.

Han SeJin (2007): Finite Element of Lamb Waves Acting Within a Thin Aluminium Plate, US Air Force Institute of Technology, Wright-Petterson Air Force Base, Ohio.

Termín odevzdání diplomové práce je stanoven časovým plánem akademického roku 2015/16

V Brně, dne

L. S.

doc. Ing. Jaroslav Juračka, Ph.D. ředitel ústavu	doc. Ing. Jaroslav Katolický, Ph.D. děkan fakulty

ABSTRACT:

In the present thesis, SHM methods used in aviation are described, and series of FEM simulations of UGW propagation in the thin-walled composite aircraft structure have been performed. For the simulation, pitch-catch SHM method is used. Experimental simulations are performed on two panels from a different material, and each of those two materials is tested with three configurations of crack and one configuration without a crack. For the simulation preprocessor MSC.Patran and two post processors MSC.Nastran and MSC.Dytran are used for comparison of results. Simulations showed that cracks in the panel are affecting velocity and amplitude of waves. In configurations with crack, velocity and amplitude are lower than in the case without a crack. In FEM simulations, post processor MSC.Nastran showed more accurate and easier data for reading for further study of UGW propagation.

KEYWORDS:

Structural Health monitoring; FEM simulation; Ultrasonic wave propagation;

ABSTRAKT:

V této diplomové práci jsou popsané SHM metody používané v letectví a dále jsou udělány MKP simulace šíření ultrazvoukových vln v celokompozitním tenkostěnném materiálu používaném u leteckých konstrukcí. Pro simulaci byla zvolena SHM metoda nazývaná pitch-catch. Simulace byla provedena na dvou různých kompozitových materiálech a každý z nich byl testován třemi různými konfiguracemi s trhlinou a jednou konfigurací bez trhliny. Jako prepocessor byl použit MSC.Patran a jako post processory byli použity MSC.Nastran a MSC.Dytran, jejichž výsledky byli na závěr porovnány. Simulace prokázali, že rychlost šíření a amplituda vln šířících se v simulovaném panelu je trhlinami ovlivněna. Při konfiguracích s trhlinami rychlost šíření i amplituda vln byli menší, než v případě bez trhliny. Jako vhodnější post processor při MKP simulacích se ukázal MSC.Nastran, jehož výsledky byli přesnější a zároveň bylo i snažší správně odečítat hodnoty dat z grafů pro podrobnější pozorování šíření vln.

KLÍČOVÁ SLOVA:

Structural Health Monitoring; MKP simulace; Šíření ultrazvukových vln

CIMRHANZL, J. *Simulation of ultrasonic wave in the composite aircraft structures.* Brno: Brno University of Technology, Faculty of mechanical engineering, Institute of aerospace engineering, 2012.40 p. Supervisor Ing. Jan Šplíchal, Ph.D.

CIMRHANZL, J. *Simulace šíření ultrazvukových vln v celokompozitních tenkostěnných konstrukcích.* Brno: Vysoké učení technické v Brně, Fakulta strojního inženýrství, 2016. 40 s. Vedoucí diplomové práce Ing. Jan Šplíchal, Ph.D

DECLARATION

I declare that I have prepared this dissertation independently, under supervision of the master's thesis supervisor. I have used no sources other than those quoted and the literature I have used has been clearly cited in the text.

Brno, 26/5/2016 ……

(author's signature)

ACKNOWLEDGEMENT

I would like to express my sincere gratitude to my supervisor Ing. Jan Šplíchal, Ph.D. I would like to thank him for his great support and guidance during this work. I would also like to thank my family for their support during my studies.

Brno, 26/5/2016 ……

(author's signature)

Contents

List of Figures:

List of Tables:

List of symbols:

C_L	[m/s]	Longitudinal wave speed
C_{L1}	[m/s]	Longitudinal wave speed for the free plate
E	[Mpa]	Young's modulus
ρ	[kg/m^3]	Density
G	[Mpa]	Shear modulus
λ	[Pa]	Lame constant
μ	[-]	Poisson's ratio
C_T	[m/s]	Transverse wave speed
ψ	[s]	Mother wavelet
t	[s]	Time
a	[-]	scale translation parameter inversely related to frequency
b	[-]	scale translation parameter associated with time
v	[m/s]	velocity of the wave

Abbreviations:

SHM	Structural Health Monitoring
UGW	Ultrasonic Guided Wave
FEM	Finite Element Method
CAD	Computer-aided drafting
FEA	Finite Element analysis

1. Structural health monitoring (SHM) introduction

In the aviation, there is a large importance in detecting damages on aircraft in order to prevent failure of the structure that can lead to an accident. Fatigue damage, hidden cracks in locations that are hard to reach and corrosion are major flaws for today's extensive fleet of aging aircraft. Traditionally structural inspections typically consist of visual inspection, and only in exceptional cases, some more advanced methods like ultrasound or other wave propagation based methods are used. In the future, these advanced methods can save lots of money to airlines. With the use of SHM methods during the maintenance inspections, airlines will decrease the downtime of their aircraft fleet by early detection of a potential damage of critical structures.

SHM systems are able to monitor the structural response of aircraft structures, detect damage in the structure and locate location and nature of the damage. In some cases, visual inspections of structures are difficult, and there is a need for complex SHM systems for providing more reliable damage detection during maintenance inspections. (1)

During the past few years, several methods for SHM have been introduced. Active SHM is using actuator for exciting the signal and sensor for transformation of the sensed signals from mechanical energy into electrical energy. This technique directly monitors structure of a material by signal, which is moving through the monitored panel and creates vibrations. Passive SHM technique does not send any waves through the material. It only monitors structural responses caused by impacts to the structure. Passive technique correlate various measurements (environmental conditions, Loads) to make interference to the probability of damage occurrence. There is also Scheduled and Unscheduled SHM. Scheduled SHM is a system which monitors the structure, and at the scheduled time, maintenance personnel check data from thy system. In the Unscheduled (automated) SHM, a system automatically initiates maintenance action.

In the case, there is importance to have a signal more precise, there are several methods how to improve the resolution of the signal. Some methods for the SHM are using modal parameters such as natural frequency, damping ratio and mode shapes. Methods, which are using these parameters are Wavelet transform, Hilbert-Huang transform, parametric system identification and peak picking. SHM method involves four basic phases which are required to be done step by step. *The first one is identification of damage existence in the structure, the second is identification of single or multiple damage location, the third is quantification of the level of damage, and the last fourth one is evaluation of structural performance.* (2)

1.1 Vibration and Wave propagation approach

Vibration Approach is used to determine location and nature of a defect in the structure. Changes in the frequency response signalize presence of damage in the structure. Vibration approach is useful for detecting widespread or extensive damage. On the other hand, when defects are small compared to the dimension of the structure, it is hard to distinguish a difference in the vibration response because they are too small.

Wave propagation approach is useful also for small hidden defects of the structure. Wave propagation can find these defects because the wavelength is much smaller than the defects. (3)

1.2 Active and Passive Techniques in SHM

Active SHM is using actuator for exciting the signal and sensor for interrogating the structural responses of the tested structure. Signals sensed by the sensor are analyzed for determination of damage of the structure. This technique directly monitors structure of a material by signal, which is moving through the monitored structure and creates vibrations. Active SHM is shown in Figure 1.

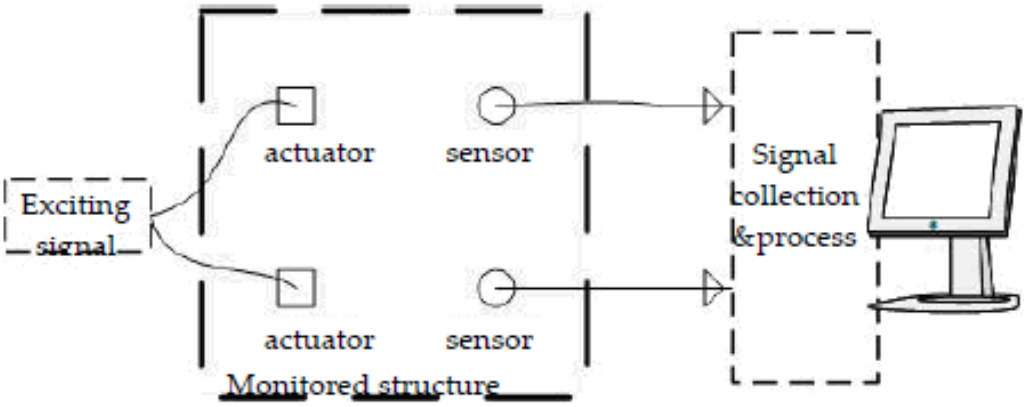

Figure 1 Active SHM (4)

Passive SHM technique does not send any waves through the material. It only monitors the structural responses caused by impacts to the structure. Passive technique correlate various measurements (environmental conditions, Loads) to make interference to the probability of damage occurrence. Passive SHM is shown in Figure 2

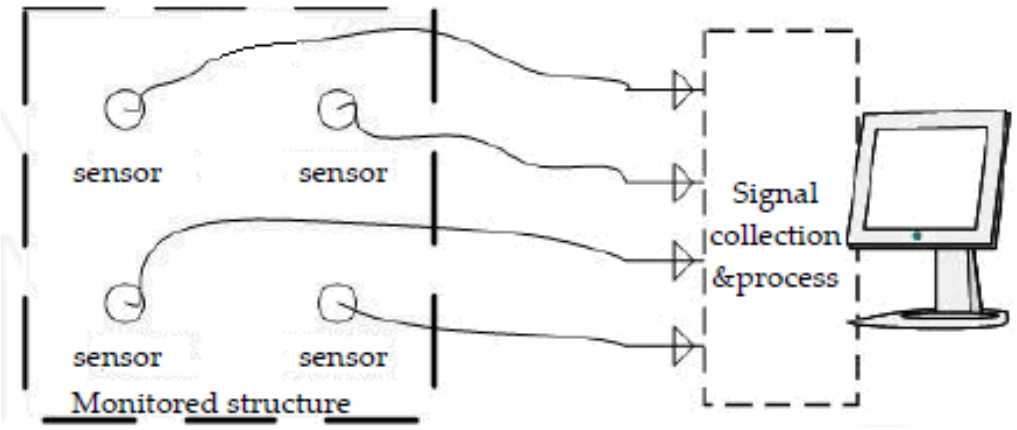

Figure 2 Passive SHM (4)

1.3 Pitch-Catch Technique

Pitch-Catch technique is an ultrasonic non-destructive technique that is based on propagation and reflection of elastic waves. The waves for this technique are generated by actuating transducer, and the response is recorded by sensing transducer. For covering the whole area, there are required various pairs of pitch-catch transducer. An example of the distribution of piezoelectric transducers in the testing panel is shown in Figure 3. The damage and its location is estimated by the examining the response of the waves. (3)

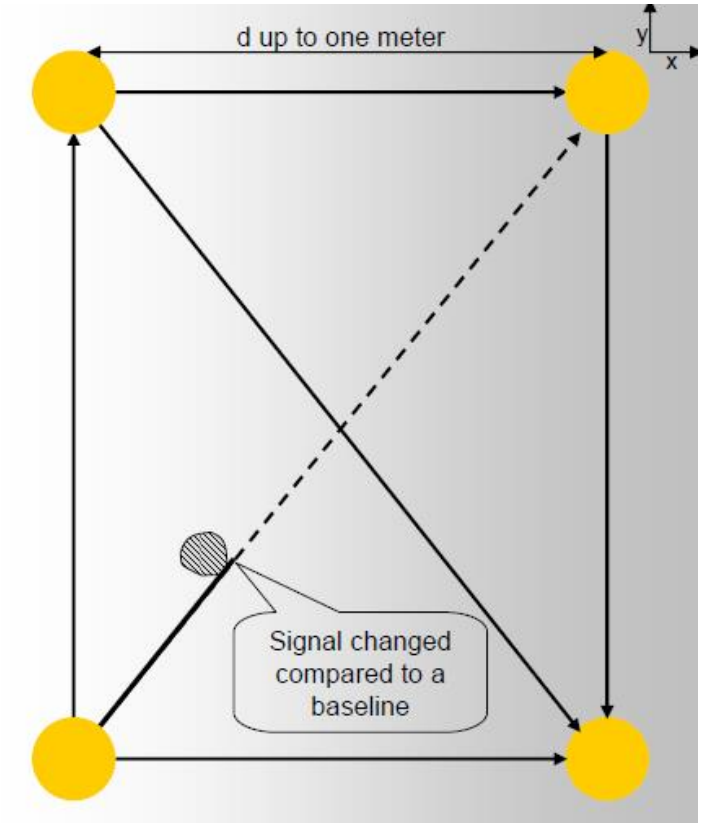

Figure 3 Pitch-Catch principle (over several patches) (5)

1.4 Puls-echo Technique

In the pulse-echo technique, the single piezoelectric transducer is placed on the panel. This transducer then works as transmitter and receiver. In this configuration transmitter sends a signal, and once the signal reaches the boundary of the panel, the echoed signal is coming back to the receiver. Signals time of the flight can be used to locate the damage, and amplitude of the received signal can be used for estimation of the severity of the damage.

The drawback of this technique is its sensitivity. Due to the longer distance which the wave has to travel, the received signal loses important information regarding to the defects on the panel. Also, the defects close to the transductor are hard to be analyzed due to interference with the excitation signal from the transductor.

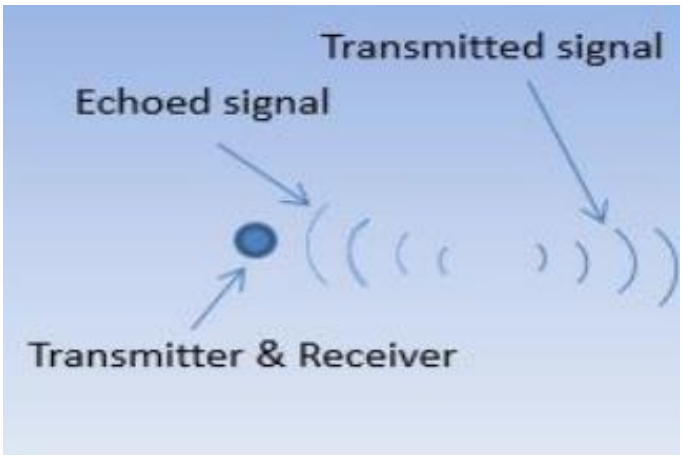

Figure 4: Pulse-echo configuration

1.5 Piezoelectric transducer

The piezoelectric transducer is a device that is capable of converting energy from one form to another. In SHM, transducers are used for changing of input energy in the form of lamb waves to electrical energy. Piezoelectric transducers can be used for both actuating and sensing of Lamb waves. A transducer that sends a wave is an actuator and transducer that receives the wave is a sensor. The voltage differential of the actuating transducer causes its radius to contract and expand. These radial displacements generate elastic waves to the material, where the transducer is mounted. The sensor in the other place receives these waves, and it causes the sensing transducer to generate voltage differentials, which are recorded. (3)

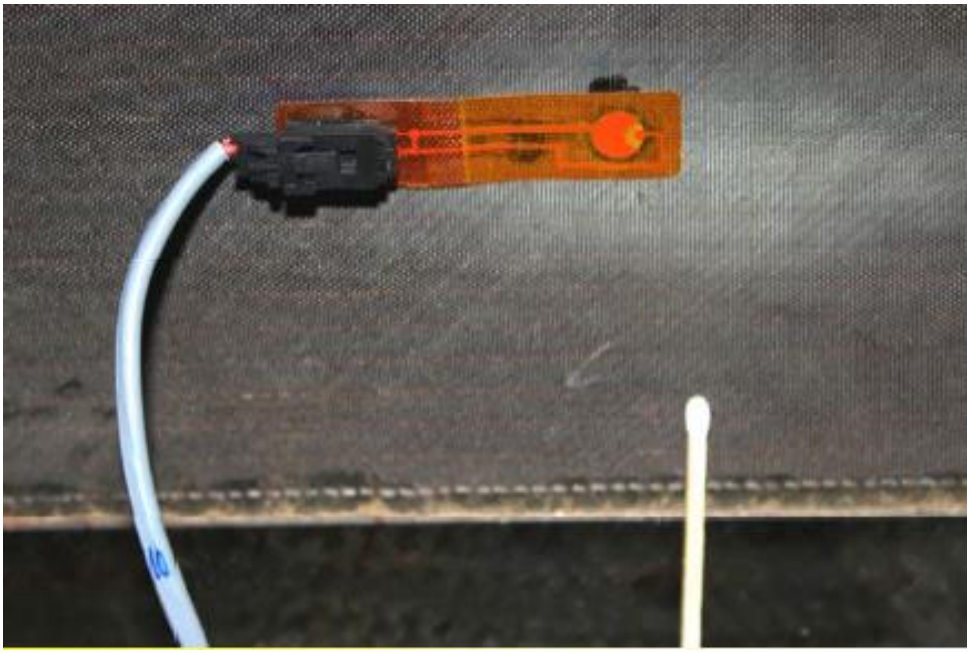

Figure 5 Acousto Ultrasoninc sensor (5)

1.5 Elastic waves

Elastic waves are waves that transmit changes in stress, and velocity inside the material and these changes influence the wave characteristics like frequency, period, phase, wavelength, amplitude of particle displacement, and wave speed.

The elastic wave consists of bulk wave or guided waves. For the SHM purpose, the guided waves are used. Guided waves consist of Rayleigh waves or Lamb waves. Rayleigh waves are free waves on the surface and are used for damage detection of surface cracks in thick structures.

1.5.1 Longitudinal Waves

Longitudinal waves are also known as pressure, compressional, or dilatational waves. This wave produces compression and rarefaction when moving through the media. Particles of wave move parallel to the direction of wave propagation.

The propagation of longitudinal wave is dependent on the density and elastic properties of a medium

The longitudinal wave speed

$$C_L = \sqrt{\frac{E}{\rho}} \tag{1}$$

- Where E is Young's modulus and ρ is density

The longitudinal wave speed for the free plate

$$C_{L1} = \sqrt{\frac{\lambda+2G}{\rho}} \tag{2}$$

- Where λ is Lame constants given by

$$\lambda = \frac{E\mu}{(1+\mu)(1-2\mu)} \tag{3}$$

- G is shear modulus

$$G = \frac{E}{2(1+\mu)} \tag{4}$$

Lame constants are function of Poisson's ratio μ and Young's modulus E

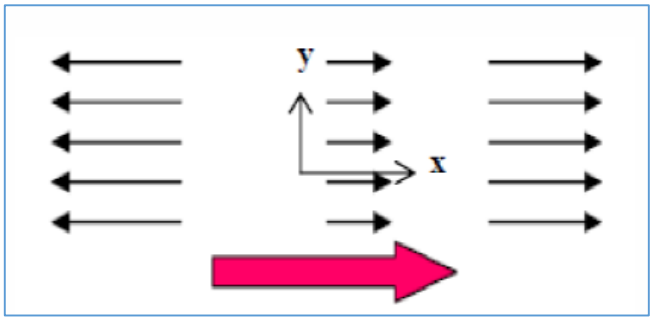

Figure 6 Longitudinal wave (3)

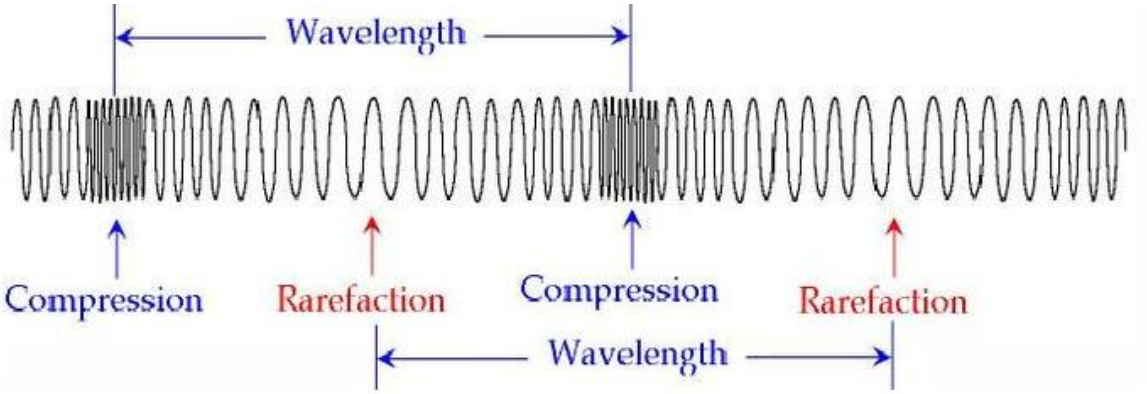

Figure 7 Propagation of Longitudinal wave in time. The wave propagate in the same direction of oscillation (6)

1.5.2 Transverse wave

Transverse waves are also known as shear waves or distortional waves. Particle motion of these waves is perpendicular to the direction of propagation.

The transverse wave speed

$$C_T = \sqrt{\frac{G}{\rho}} \tag{5}$$

- Where *G* is shear modulus and ρ is density

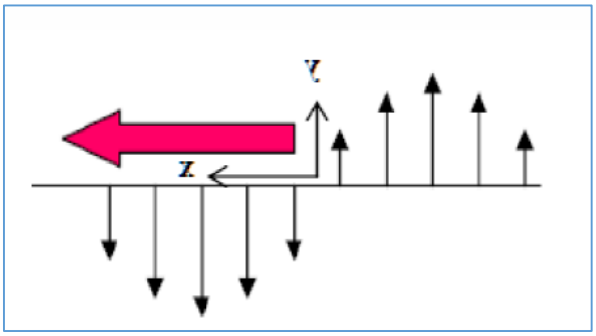

Figure 8 Transverse wave (3)

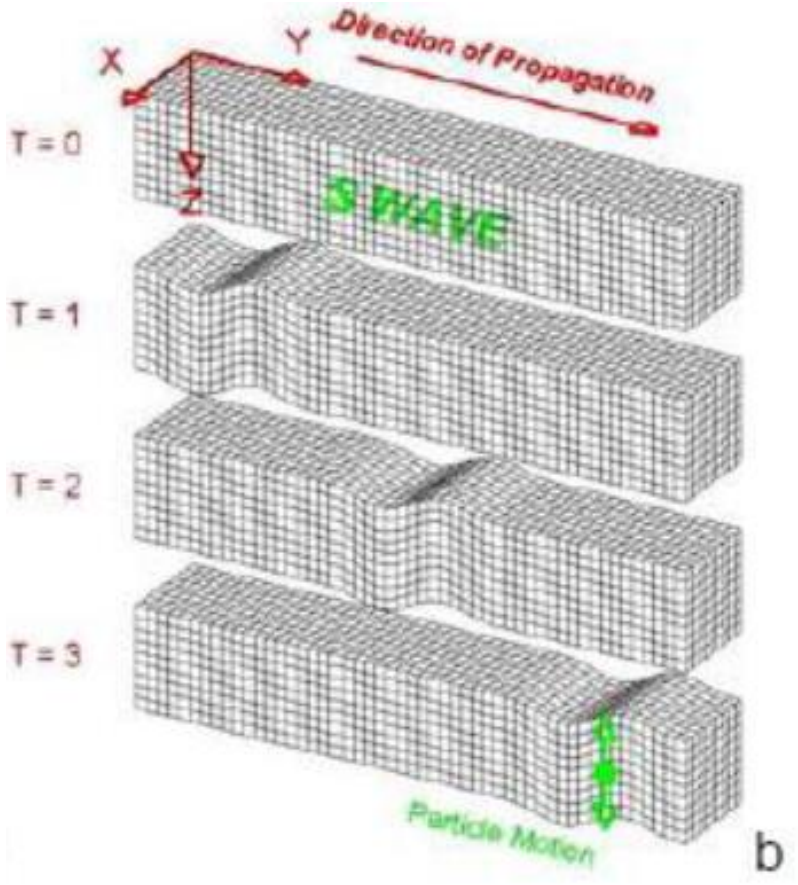

Figure 9 Propagation characteristics of Transverse wave in time (7)

1.5.3 Lamb waves

Lamb waves are waves of plain strain in a free plate. Lamb waves are useful for damage detection in plate and shell structures. The advantage of Lamb waves is that they can propagate over large distances. It provides interrogation through the whole thickness of the structure, and it allows detecting of internal defects in thin materials. (3)

Lamb waves result from the conversion between transverse and longitudinal modes. Because Lamb waves are waves of plane strain, there are considered only displacements through the thickness (y-direction) and in the direction of wave propagation (x- direction). For the Y-direction, it is a Transverse wave and for x-direction, it is a Longitudinal wave. Propagation of Lamb waves depends on density, elastic properties and geometric structure of the used media.

Lamb waves have several modes. In this thesis, only symmetric mode S_0 and antisymmetric mode A_0 is considered. Symmetric modes have opposite vector of speed in the Y axis, and antisymmetric has the same vector of speed in Y axis (see Figure 10 below). Symmetric waves have a lower amplitude than antisymmetric waves. In this thesis where excitation frequency of 100KHz frequency is used, symmetric waves have higher speed than antisymmetric waves according to Figure 11.

Figure 10 Symmetric and Antisymmetric modes of Lamb wave (8)

Lamb wave speed-frequency relationship between symmetric and antisymmetric modes shown in Figure 11.

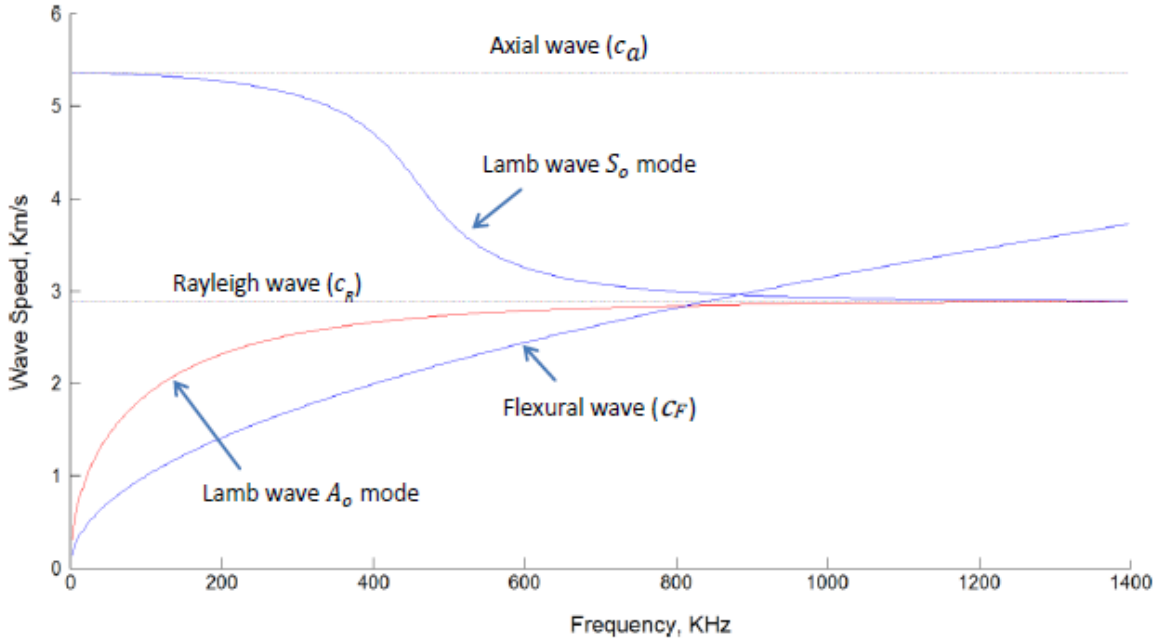

Figure 11 Wave speed dependency of Lamb wave modes on frequency (7)

2 Finite Element Method (FEM) usage for structural health monitoring

For the purpose of modeling of the ultrasonic wave propagation in isotropic solid media, Finite Element Method (FEM) is used for better understanding of the interaction of wave with the material. FEM model used for the modeling must be optimized properly in order to obtain the solution closer to the exact one. For the study of the change in the shape of the incident wave, amplitude, and frequency with respect to the change in length of element and time steps, several programs can be considered for usage. (9)

The advantage of ultrasonic testing is that it is a Non-Destructive testing. It can be widely used for characterization of materials and detection of defects in materials. Understanding of ultrasonic wave propagation and its capability is essential for the proper determination of material characteristics or detection of defects. For the simulation of the waves, FEM can be used.

2.1 MSC. Patran

MSC Patran is a pre/post processing software used for Finite Element Analysis, providing solid modeling, meshing, analysis setup and post-processing for multiple solvers including MSC Nastran, Marc, Abaqus, LS-DYNA, ANSYS, and Pam-Crash.

Patran provides a rich set of tools that streamline the creation of analysis ready models for linear, nonlinear, explicit dynamics, thermal, and other finite element solutions. From geometry cleanup tools that make it easy for engineers to deal with gaps and slivers in CAD, to solid modeling tools that enable creation of models from scratch, Patran makes it easy for anyone to create FE models. Meshes are easily created on surfaces and solids alike using fully automated meshing routines, manual methods that provide more control, or combinations of both. (10)

2.2 MSC. Nastran

MSC Nastran is a multidisciplinary structural analysis application used by engineers to perform static, dynamic, and thermal analysis across the linear and nonlinear domains, complemented with automated structural optimization and award winning embedded fatigue analysis technologies, all enabled by high performance computing.

MSC Nastran is based on sophisticated numerical methods, the most prominent being the Finite Element Method. Nonlinear FE problems may be solved either with built-in implicit or explicit numerical techniques. A number of optimization algorithms are available, including MSCADS and IPOPT. The fatigue capability in MSC Nastran has been developed jointly by nCode International Ltd. and MSC Software. (10)

MSC.Nastran Explicit Nonlinear (SOL 700) offers a powerful explicit solution to simulate complex Fluid Structure Interaction (FSI) problems and analyze dynamic events of short duration with severe geometric and material nonlinearities.

MSC.Nastran SOL 700 allows users to work within one common modelling environment using the same Bulk Data interface. The Nastran models can be used for explicit applications such as crash, crush, and drop test simulations. This dramatically reduces the time spent to build different models for implicit and explicit analysis and prevents users from making mistakes because of unfamiliarity between different programs (11)

2.3 MSC.Dytran

MSC.Dytran is an explicit finite element analysis (FEA) solution for simulating short-duration events like impact and crash, and to analyze the complex nonlinear behaviour that structures undergo during these events. MSC.Dytran enables users to study the structural integrity of designs to ensure that final products stand a better chance of meeting customer safety, reliability, and regulatory requirements.

MSC.Dytran delivers a structural, material flow and coupled FSI analysis capabilities in a single package. MSC.Dytran uses a unique coupling feature that enables integrated analysis of structural components with fluids and highly deformed materials in one continuous simulation. (10)

3. Methods for modifying signals in SHM

These techniques are used for extracting useful information from experimental data. The first step is the noise reduction because piezoelectric sensors are very sensitive to vibrations. Fortunately, the frequencies which are used in SHM are very high (100 KHz to MHz range) in comparison to the usual noise source. Because the piezoelectric sensors receive all random noise, noise reduction must be used to have a clear data for further analyses.

Wavelet Transform

In the field of the wavelet transform, there was a significant development in last decade. Now applications of wavelet transform range from signal processing to image compression, from denoising to matrix multiplication, etc.

Collected data could be represented in the time or frequency domain by the use of Fourier series. The main characteristic of the wavelet transform is its adaptive nature. It breaks a signal into different frequency bands. The biggest advantage of wavelet transform in comparison with other signal transform is its windowing technique with variable size window (Figure 12). The wavelet transform is capable of utilizing long time intervals, where precise low-frequency information is needed, and short time intervals for high-frequency information. It means that *for high frequency, wavelet transform provides large bandwidth and good time localization, and for smaller frequencies it uses smaller bandwidth with better frequency localization* (2).

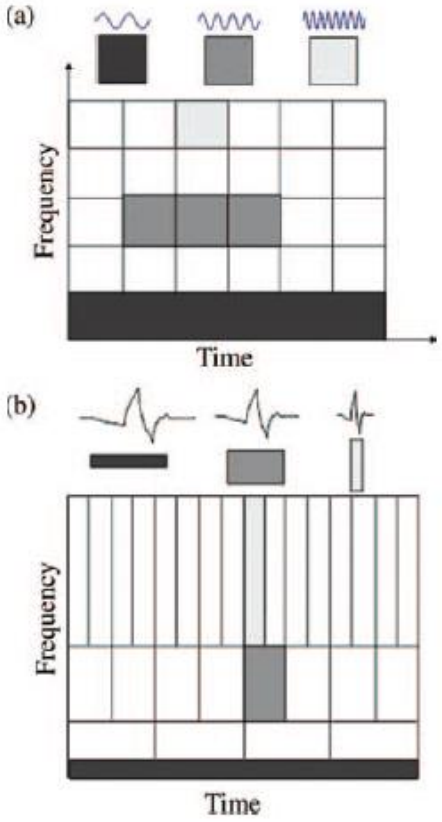

Figure 12: a) short time Fourier transform with fixed width of window and b) wavelet transform with variable width of window (1)

Wavelet transform can be used in many disciplines, and one of the biggest potentials of it is in the field of SHM and damage detection.

The wavelet transform of signal x(t) is expressed as (12)

$$C(a,b) = \int x(t)\psi_{a,b}(t)dt \quad (6)$$

Where $\psi_{a,b}(t)$ is defined as,

$$\psi_{a,b}(t) = \frac{1}{\sqrt{a}}\psi\frac{t-b}{a} \quad (7)$$

In equation (6) $C(a,b)$ are wavelet coefficients. ψ is the mother wavelet, and *a* and *b* are scale and translational parameters. The wavelet coefficients are functions of these two parameters (*a, b*). This means that the wavelet transform of a one dimensional signal is a two dimensional function. The Parameter *a*[1] is inversely related to frequency and parameter *b* is associated with time. In a wavelet analysis, dilation in time domain corresponds to a contraction in frequency domain, and it is controlled by the parameter *a,* which can be called scale parameter. In Figure 13, there is comparison of different *a* coefficients.

[1] Parameter *a* changes the frequency domain and also the time domain

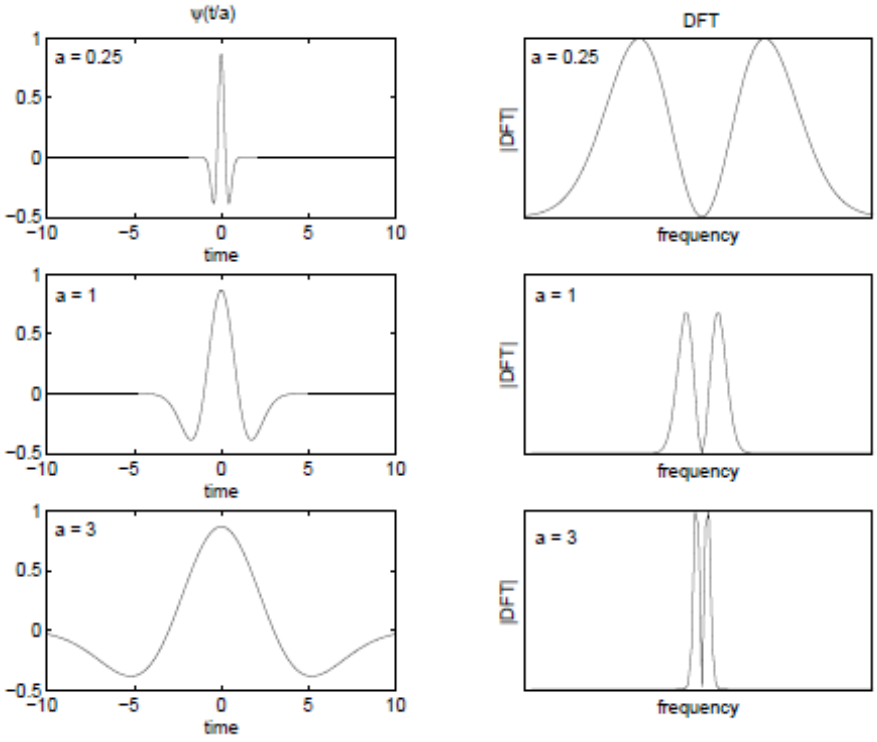

Figure 13 : Time domain function and its corresponding discrete Fourier transform for different values of the parameter ***a*** *(2)*

Admissibility condition for wavelets:

The wavelet must comply two basic properties,

1. Wavelet must be oscillating with a zero mean

$$\int \psi(t)dt = 0 \tag{8}$$

In the frequency domain, it means that the zero frequency component of the frequency response $\psi(\omega)$ of the wavelet must be zero

$$\psi(\omega = 0) = 0 \tag{9}$$

2. For possibility of reconstruction of the function from its wavelet transform, this condition must also be accomplished

$$C_\psi = \int \frac{|\psi(\omega)|^2}{\omega} d\omega < \infty \tag{10}$$

Applications of wavelet transform

The wavelet transform is useful in identifying changes in the frequency of a signal as the time evolves. In the wavelet transform, the number of ridges is proportional to the number of cracks. Furthermore, it can reveal the location and the size of the crack. *Damage of machinery parts can be also predicted by observing the changes in the wavelet coefficients of the wavelet-transformed vibration signal* (1)

It can be for example used for detecting delamination in composite structures of aircraft. The SHM system is using piezoelectric sensors which are able to transmit a signal through the

structures and analyze the responses of material. Damage detection is done by observing the signal energy in a wavelet scalogram.

Empirical mode decomposition and Hilbert-Huang Transform

Empirical mode decomposition and Hilbert-Huang Transform is a method for non-stationary and non-linear time series analysis. A method for SHM consists of extracting the modal responses from the measured input-free responses by a numerical filtering procedure. These modal responses are called intrinsic mode function. Data from the intrinsic mode function are then used to form an analytic function using the Hilbert transform. Values from the Hilbert transform are then used for calculating the corresponding frequencies, damping ratios, and relative mode shapes. Extraction of intrinsic mode function from the data is sensitive to the filtering process. In the study, it was found difficult to calculate reliable values of the modal parameters (2)

Parametric System Identification

Parametric System Identification is another method which is used for estimation of modal parameters. There are two categories of parametric system identification. The fisrs one is parametric system identification and the second one is non-parametric system identification.

Parameters of interest in parametric system identification are dumping ratio, natural frequency, and mode shapes. The system is defined by an assumed linear difference or a differential equation. These equations have some unknown parameters which have to be estimated from the available data.

In non-parametric system identification approach, the identification starts from linear time-invariant assumption and the available input-output data.

General steps for the system identification are at first identification of variables of interest, development of the mathematical model, estimating the parameters of the model, and validation of the model. (2)

4 Simulation of ultrasonic guided wave propagation with FEM software

The practical part of the thesis is focused on the comparison between two approaches of application of commercial FEM software system for modeling ultrasonic guided waves (UGW) propagation in composite aircraft structure. For the first approach MSC.Patran/MSC.Dytran is used. For the second approach MSC.Patran/MSC.Nastran-SOL700 is used. For the purpose of simulation of UGW propagation in composite structures, a panel with the configuration containing actuator, sensor and different cracks as shown in Figure 14 and Figure 15 is used. On the panel, an actuator for excitation of UGW and sensor for sensing of UGW are placed. Material properties of used panels for simulation are shown in Table 1, material properties of piezoelectric transductors are shown in Table 2.

The panel is tested in four configurations:

- Without crack
- Crack with angle of 90^0 to propagating UGW
- Crack with angle of 0^0 to propagating UGW
- Crack with angle of 45^0 to propagating UGW

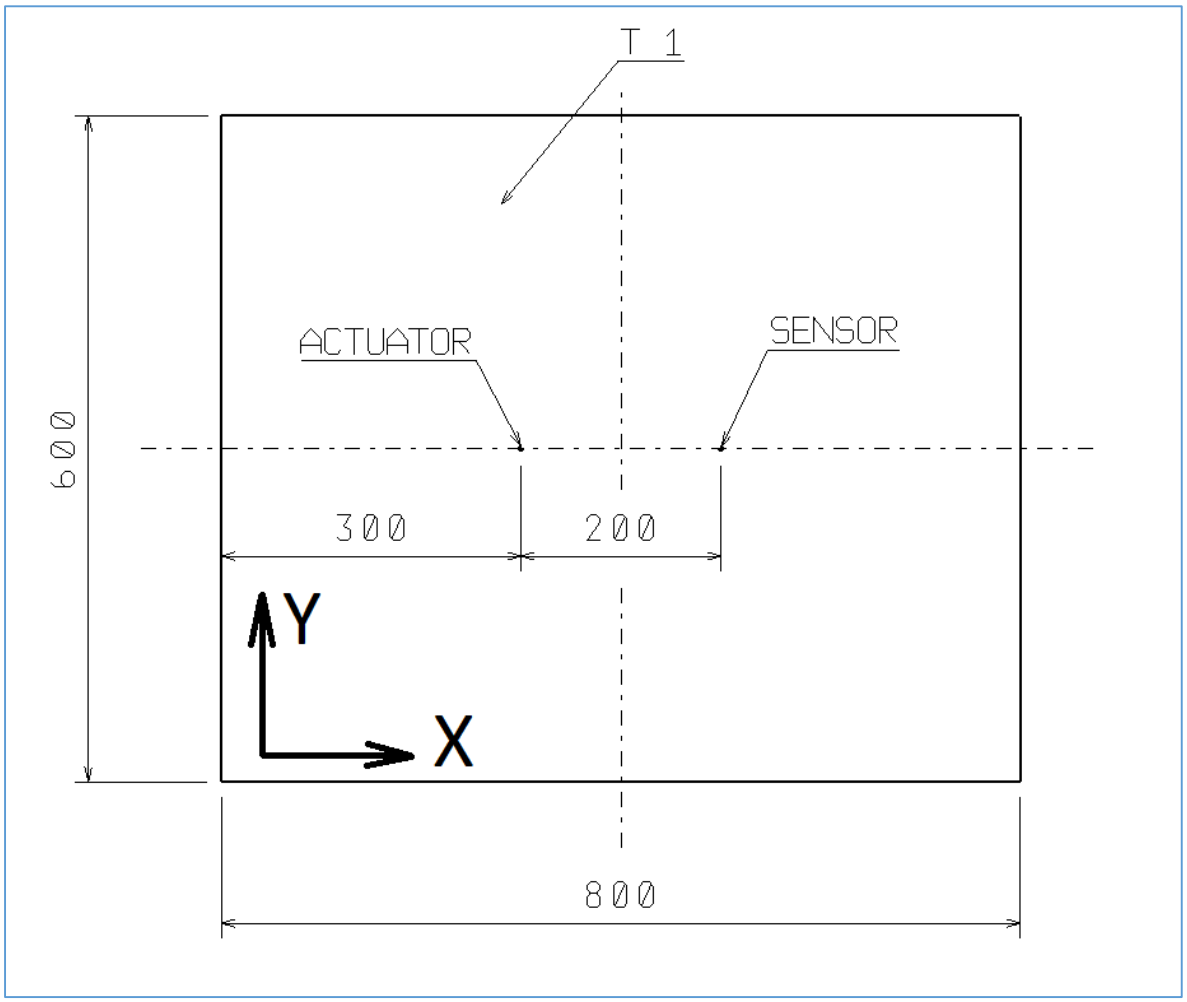

Figure 14 Panel with coordinate system and used actuator-sensor configuration without crack in [mm]

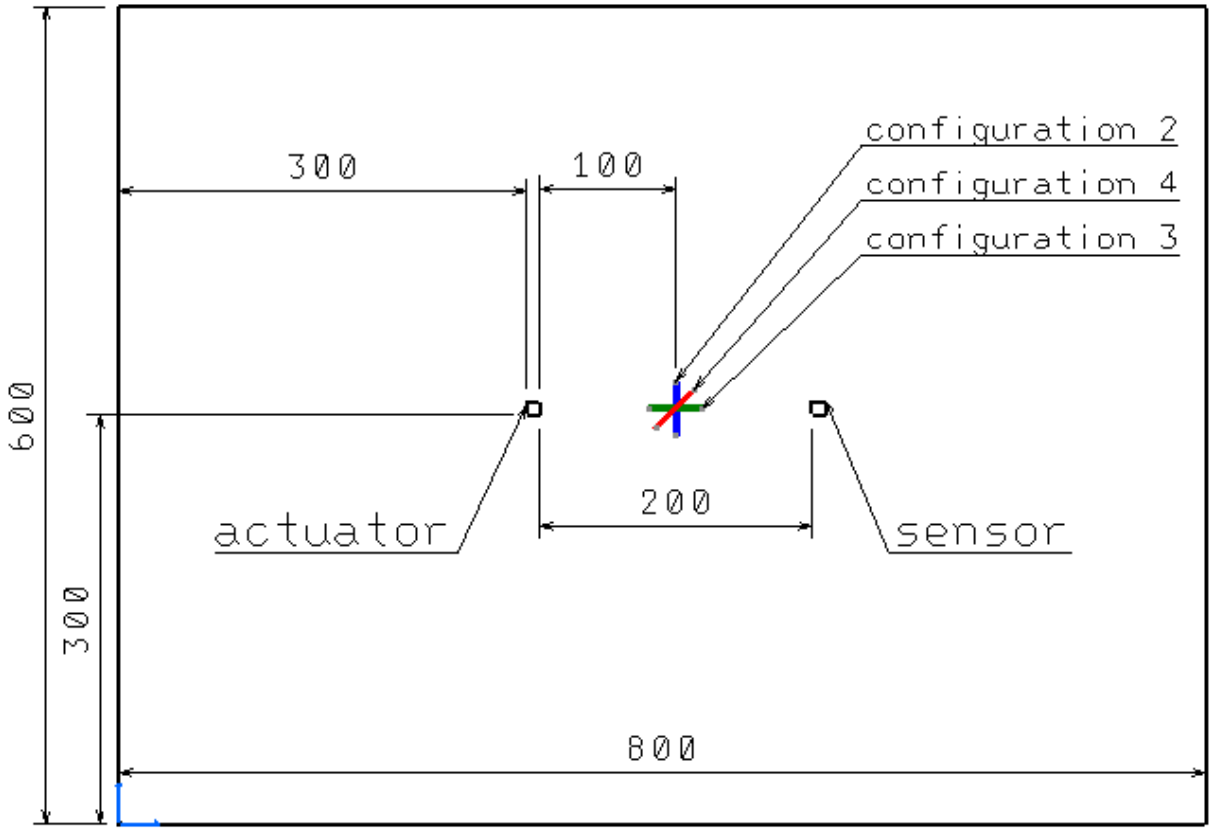

Figure 15 panel with three configurations of used cracks in [mm]

		composite [0]12	**composite [-45°/0°/45°/45°/0°/ -45°/-45°/0°/45°]s**
Material	-	(HITEX 33 6K/E7K8)	(HITEX 33 6K/E7K8)
Young's modulus	E1	125 485 Mpa	125 485 Mpa
	E2	8 618 Mpa	8 618 Mpa
Shear modulus	G12	5 400 Mpa	5 400 Mpa
	G31	5 400 Mpa	5 400 Mpa
	G23	5 400 Mpa	5 400 Mpa
Poisson's ratio	μ	0,31	0,31
Mass density	ρ	1 580 kg/m^3	1 580 kg/m^3
thickness of layer	-	0,145 mm	0,145 mm
thickness of panel	-	1,74 mm	2,61 mm

Table 1 Material properties of used panels

Young's modulus	E	32 000 MPa
Poisson's ratio	μ	0,31
Mass density	ρ	7 850 kg/m^3
Dimensions	-	3x3x2 mm

Table 2Material properties of used piezoelectric transductors

The whole model for simulation is created in MSC.Patran. The panel is modeled using 2D QUAD4 elements (2D quadrangle element) with the size of 1 mm^2 for one element shown in Figure 16(a). Sensors and actuator are modeled by 3D elements HEX8 (3D element with six surfaces) with the size of 1 mm^3 for one element shown in Figure 16(b) and Figure 17. Detailed models of used configurations of cracks are shown in Figure 18.

For the simulation, element size of 1 mm^2 is estimated from similar simulations. For the proper simulation, it is appropriate to use at least ten nodes for one wavelength (3)

Another important problem is a selection of proper time step. Long time-step leads to lower precision of results and on the other hand short time-step can lead to wasting of calculation time without effect on results. The maximum time step Δt=1.5E-8 is estimated from similar simulation.

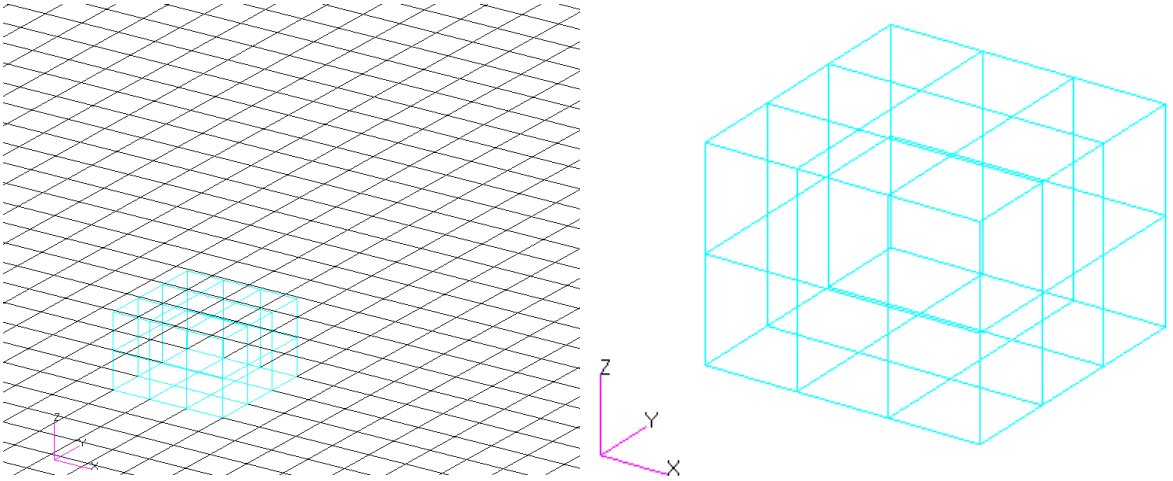

(a) (b)

Figure 16 (a) detailed view of QUAD4 elements in 800x600 mm board, (b) actuator 3x3x2mm modeled by HEX8 elements

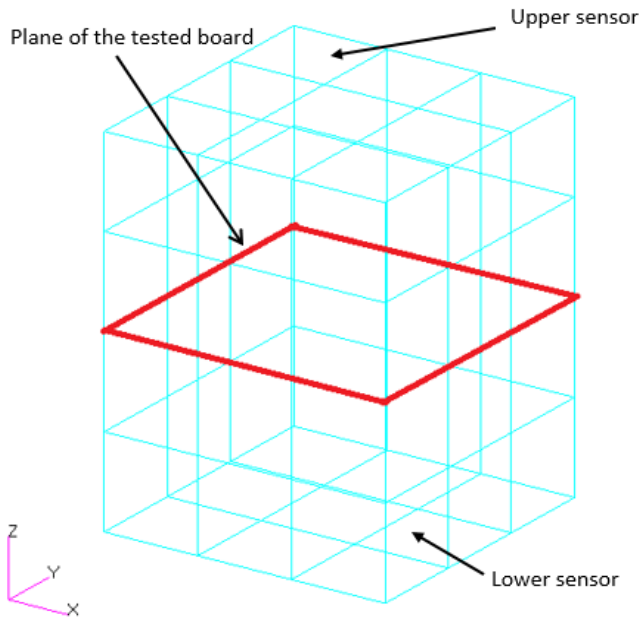

Figure 17 2 sensors 3x3x2mm placed on the top and bottom side of the board modeled by hexa elements

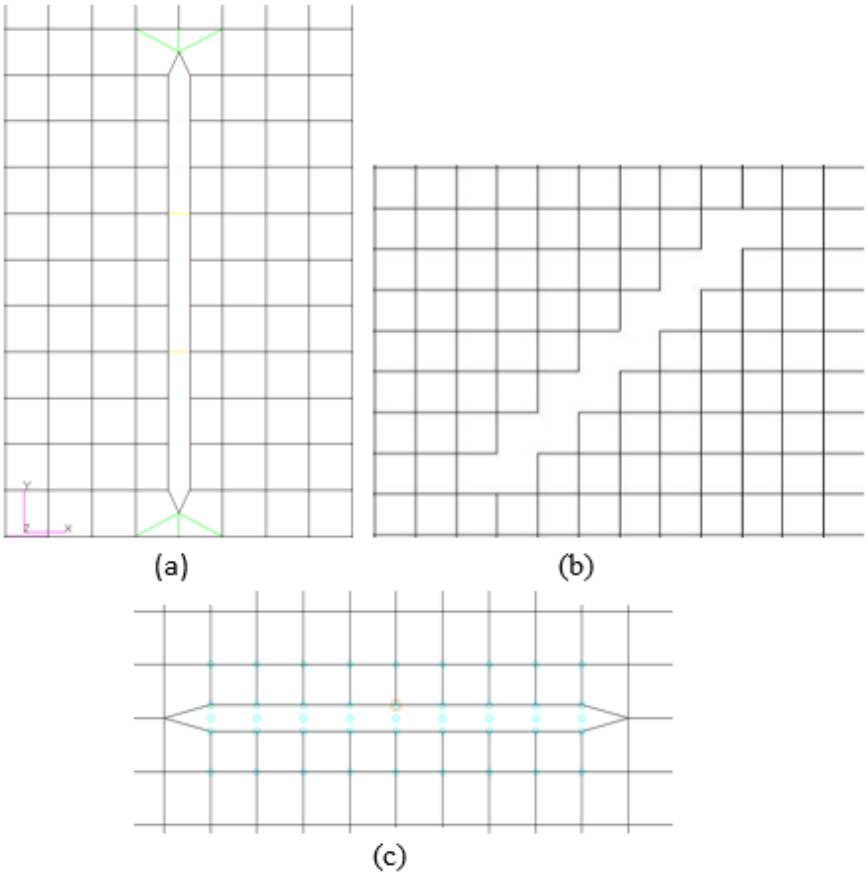

Figure 18 (a) crack 10x0.5mm, 90° angle, in the panel between actuator and sensor, (b) crack 10.6x1.4mm, 45° angle, in the panel between actuator and sensor (c) crack 10x0.5mm, 0° angle, in the panel between actuator and sensor

The UGW excited by actuator are simulated by three sinusoidal signals normalized by Gauss distribution with the frequency of 100 kHz.

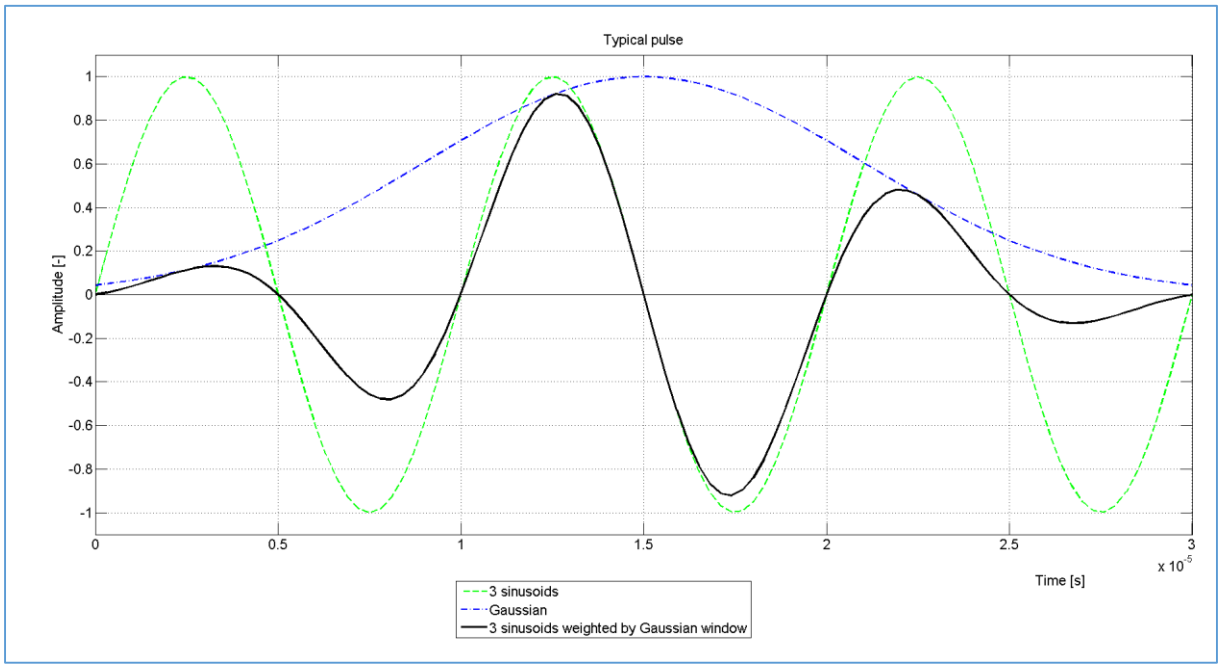

Figure 19 3 sinusoids weighted by Gaussian window scaled to amplitude one

For the purpose of initiating UGW in the simulation, excitation velocity of the actuator (shown in Figure 20(b)) is needed. It is obtained by derivation of excitation amplitude from Figure 19(a)

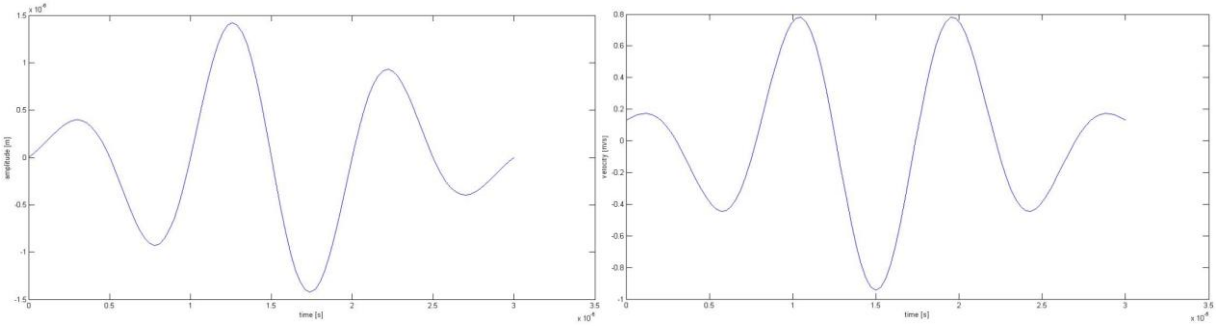

(a) (b)

Figure 20 (a) excitation amplitude, (b) excitation velocity

Data of velocity and time are applied in MSC.Patran to the upper surface of actuator perpendicular to the surface (in Z-axis) as shown in Figure 21 and Figure 22.

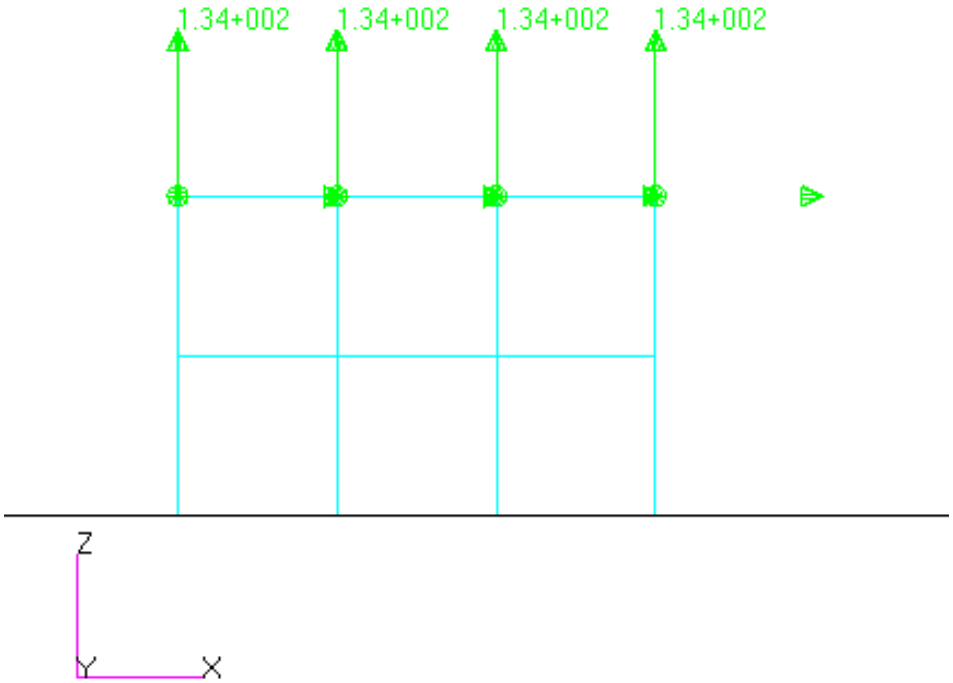

Figure 21 velocity load on actuator

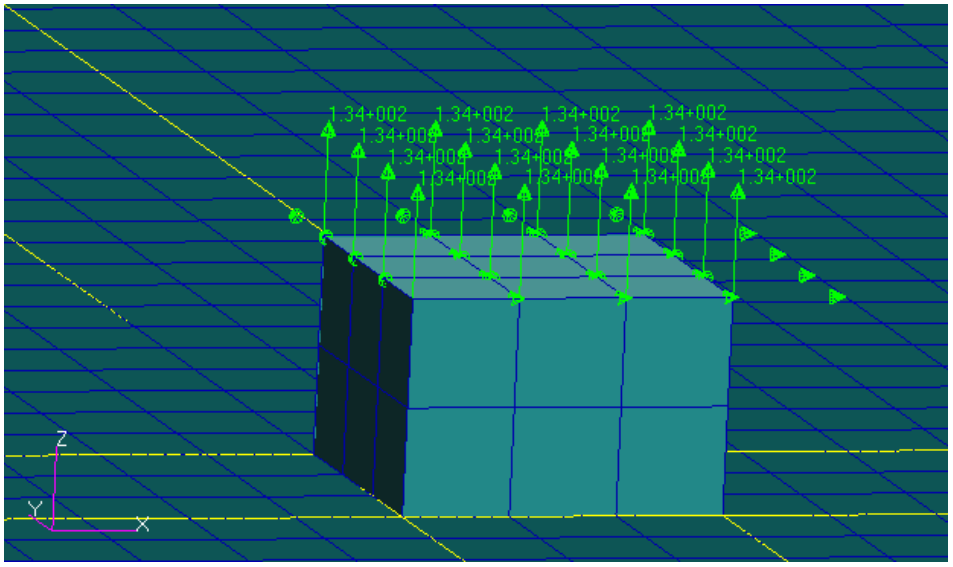

Figure 22velocity load on actuator in 3D view

4.1 FEM results

Simulations results in the recording of nodes displacement in time (at Actuator and Sensor). In the approach with post processor MSC.Dytran, velocity-time dependency is recorded and then it needs to be transformed (using integration) into displacement-time dependency by Matlab or another suitable program for this operation. With post processor MSC.Nastran(SOL700) user can select immediately in results window required data. In this case, displacement-time dependency.

In the plots, data for symmetric and antisymmetric waves are scaled to the maximum amplitude equal to one separately for further study.

$$Amplitude\ s_t = Amplitude_t \left(\frac{1}{MAX\ (Amplitude)}\right) \qquad (12)$$

Where:

- Amplitude s_t scaled amplitude in time t (max amplitude equal to 1)
- $Amplitude_t$ amplitude in time t
- Max(Amplitude) max. amplitude value during whole simulation

Data for lower and upper sensor are computed by subtraction of velocities in surfaces. 2-1 for upper sensor, 3-1 for lower sensor, and 2-1 for actuator as shown in Figure 23

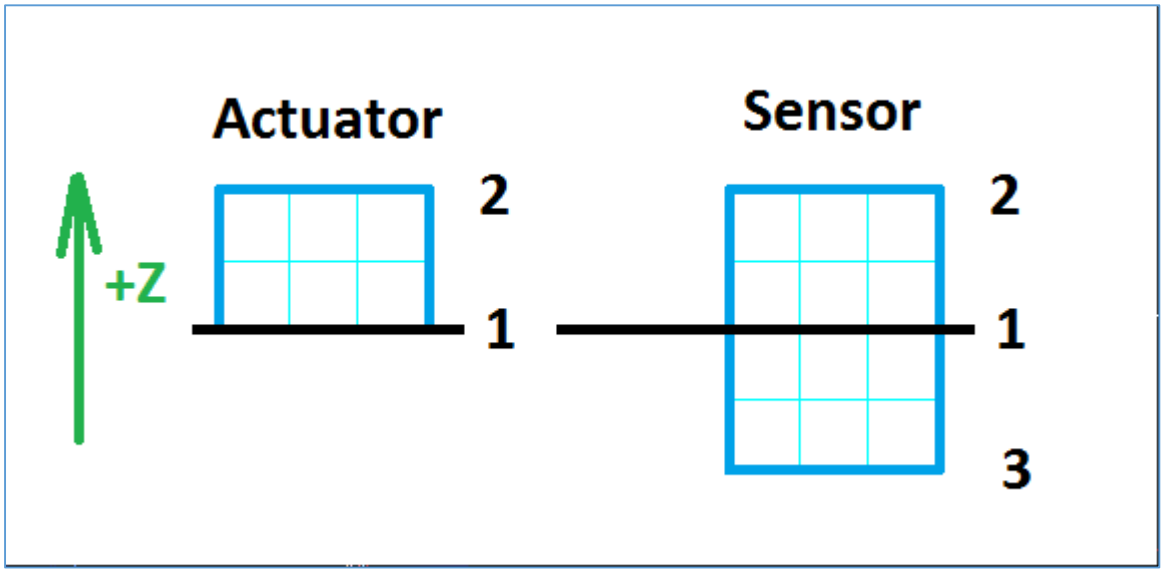

Figure 23 actuator and sensor surface numbers

4.1.1 MSC.Patran/MSC.Dytran approach

The panel, actuator, and sensors are modeled in pre processor MSC.Patran. Execution control parameters used for simulation are shown in Table 3, and output requests in Figure 24. As a post processor, MSC.Dytran is used. In this case, velocity-time dependency is recorded, and results are transformed into displacement-time dependency and plotted by Matlab.

integer memory size	200000000	-
float memory size	1000000000	-
end time	0,0002	s
time-step size at start	0,5e-7	s
minimum time step	1,5e-8	s
maximum time step	1,5e-7	s

Table 3 Execution Control parameters in MSC.Nastran used for simulation

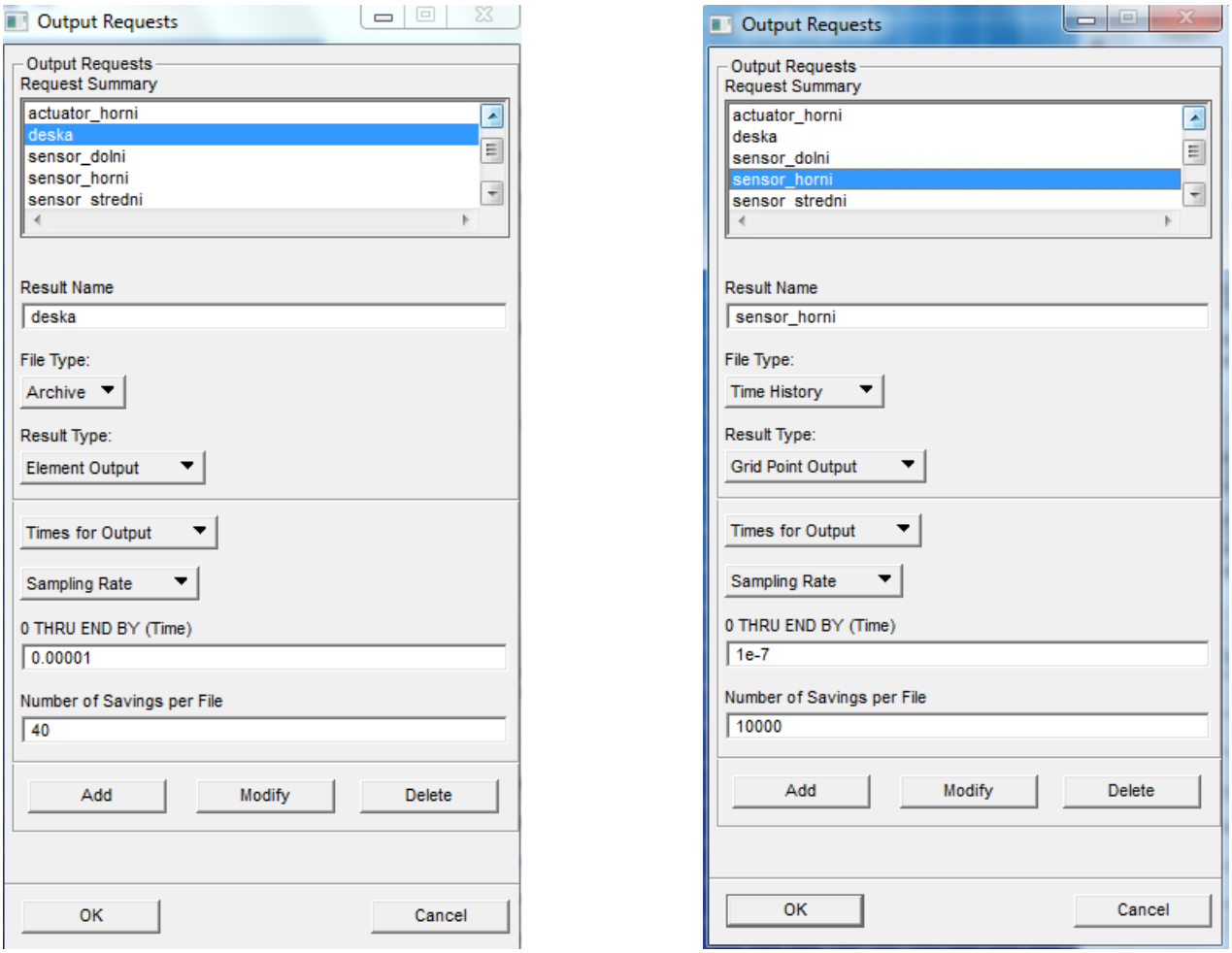

Figure 24 (a) output requests for piezoelectric transductors and panel elements (b) output requests for top and bottom nodes of piezoelectric transductors

For the analyzation of symmetric and antisymmetric waves, Matlab program is used. The main goal is to study the velocity of the antisymmetric and symmetric waves in different configurations of crack and used material. The Secondary goal is to observe the changes of maximum amplitude (scale) of displacements of symmetric and antisymmetric waves caused by a crack. Analyzed data are compared in Chapter 3.1.3 with data from Nastran Explicit Non-linear (SOL700).

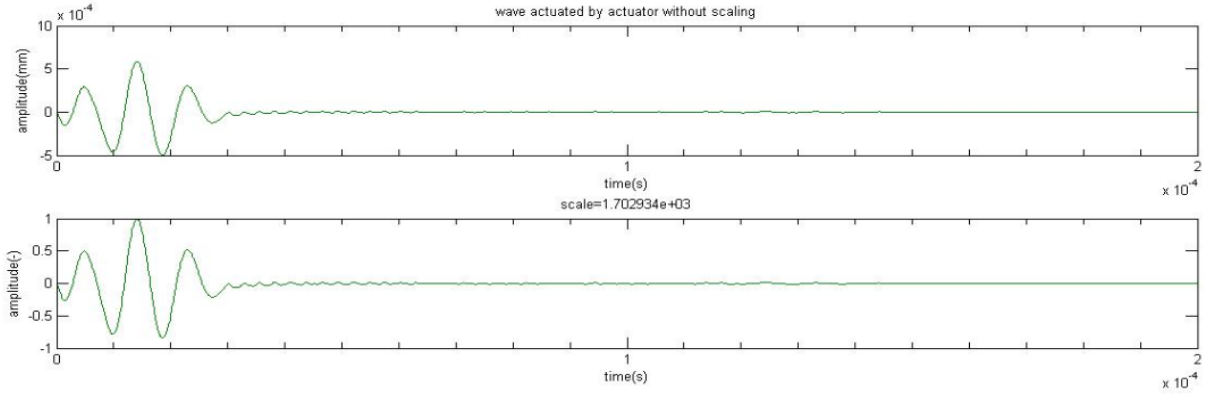

Figure 25 excitation amplitude of wave from actuator

Configuration 1: panel without crack

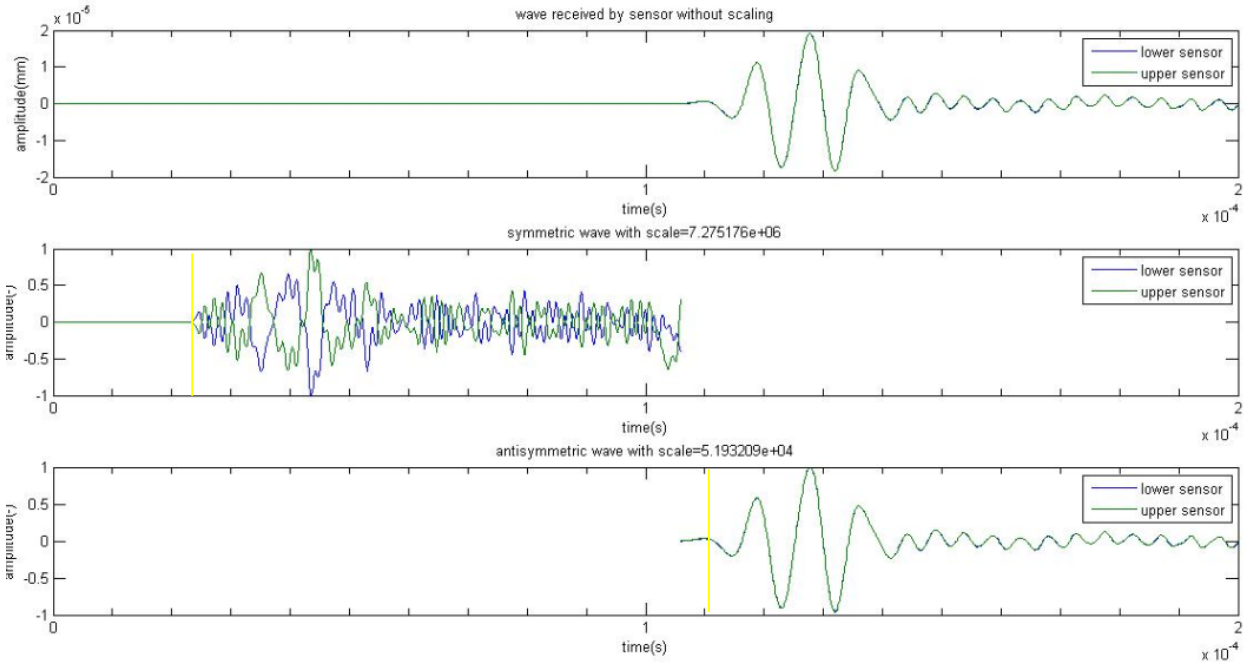

Figure 26 wave propagation in composite panel [0]12 without crack

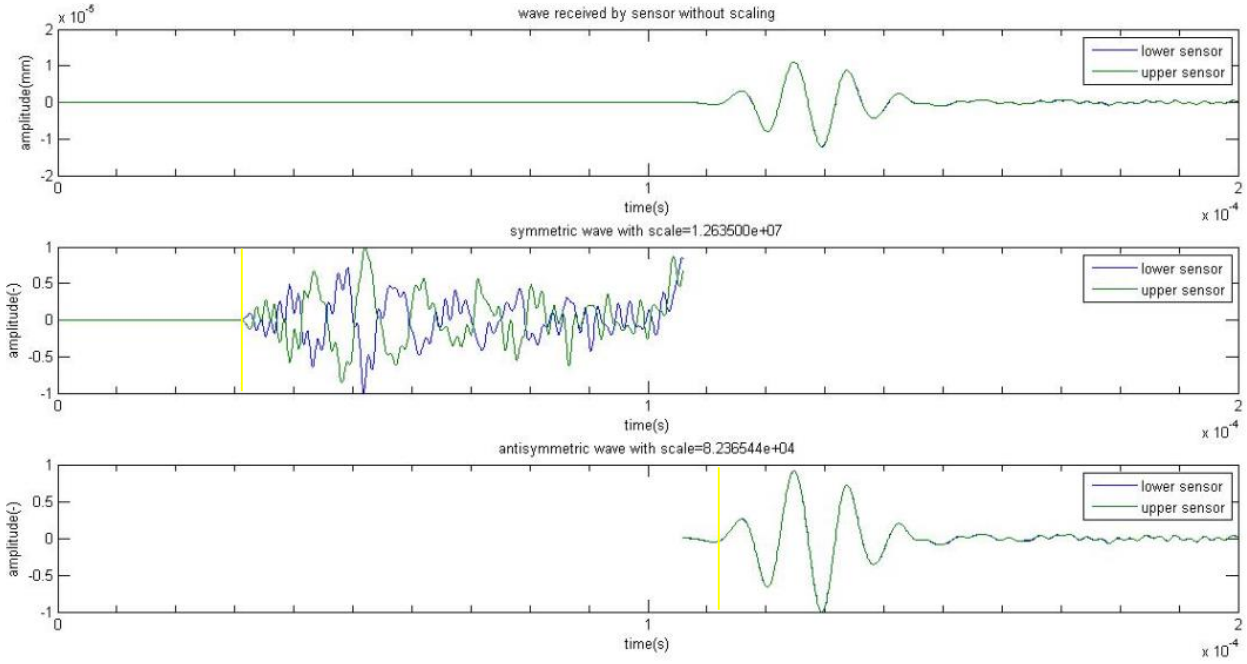

Figure 27 wave propagation in composite panel [-45°/0°/45°/45°/0°/ -45°/-45°/0°/45°]s without crack

Configuration 2: panel with a crack with angle of 90^0 to propagating UGW

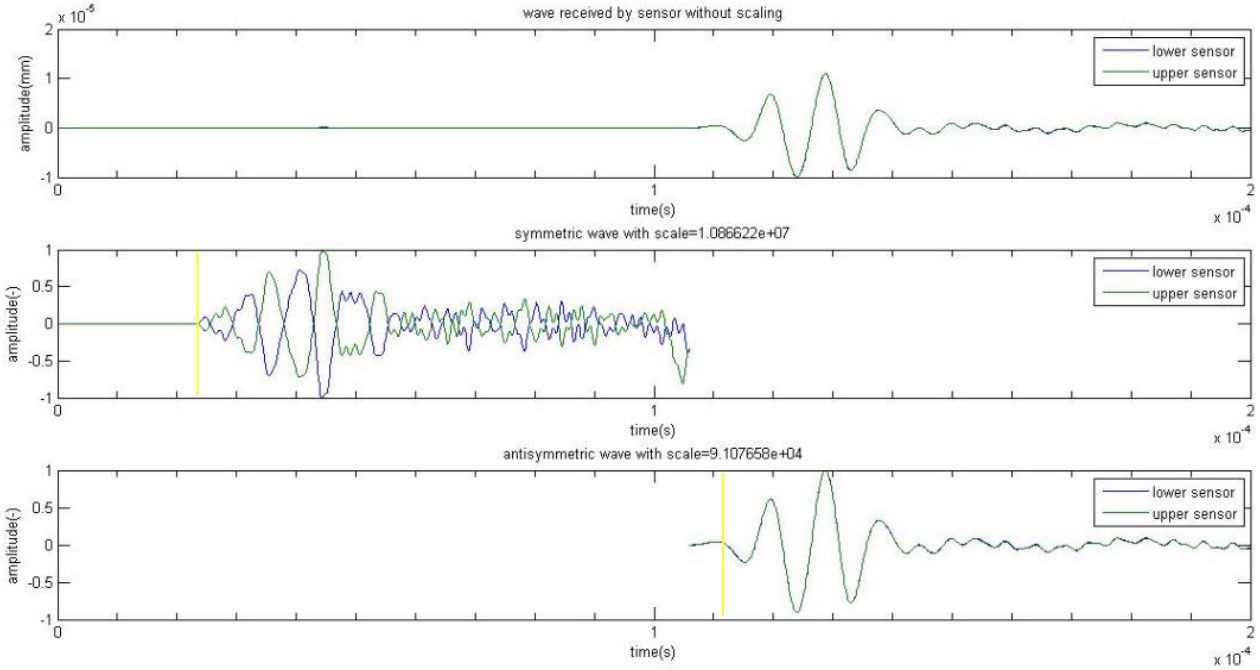

Figure 28 wave propagation in composite panel [0]12 with crack angle of 90^0 to propagating UGW

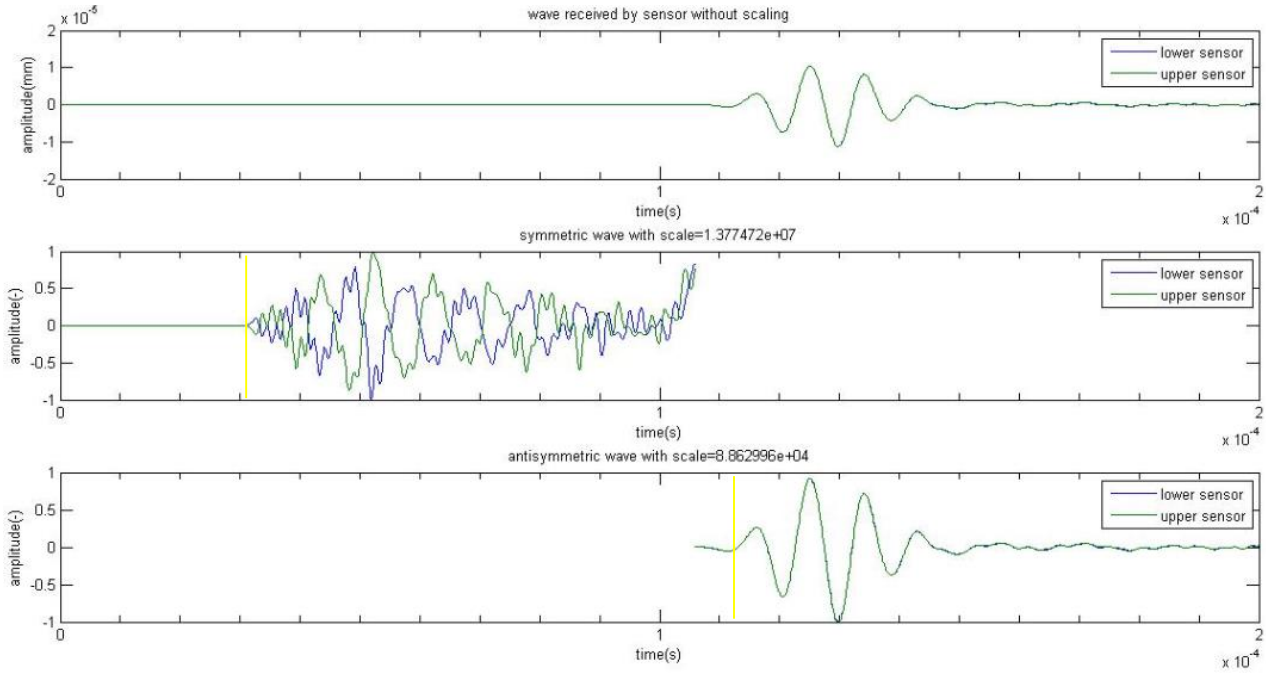

Figure 29 wave propagation in composite panel [-45°/0°/45°/45°/0°/ -45°/-45°/0°/45°]s with *crack angle of 90^0 to propagating UGW*

Configuration 3: panel with a crack with angle of 0^0 to propagating UGW

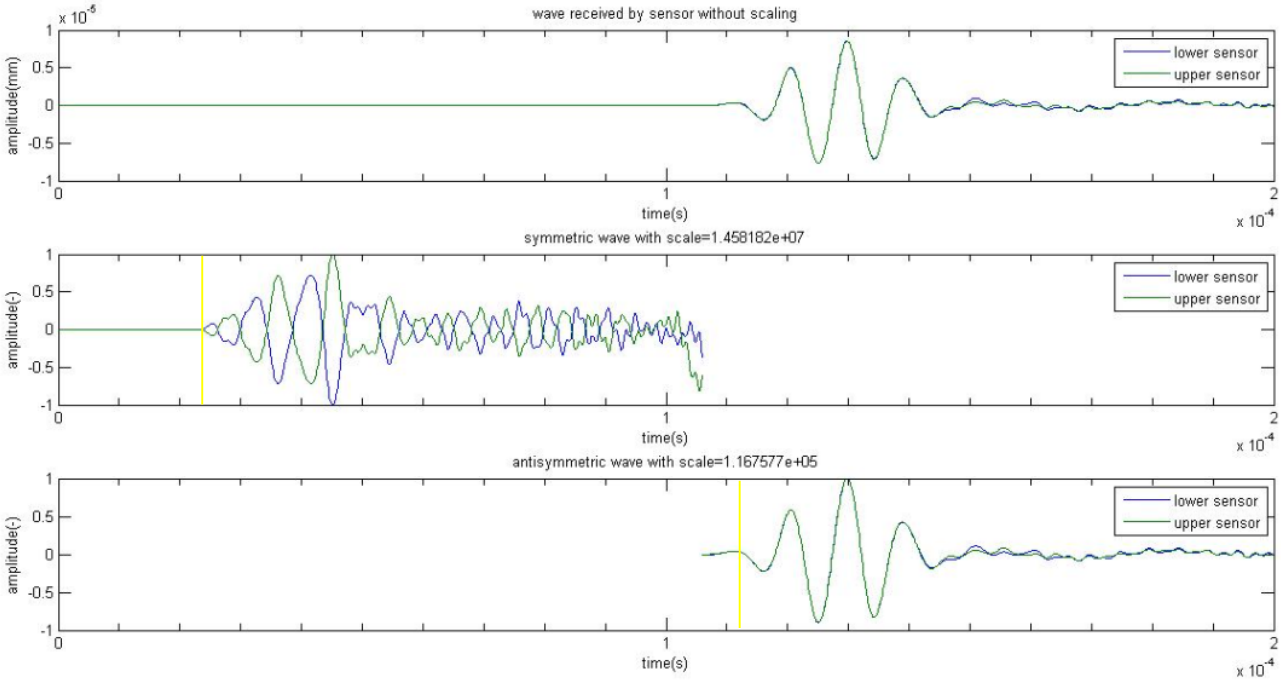

Figure 30 wave propagation in composite panel [0]12 with crack angle of 0^0 to propagating UGW

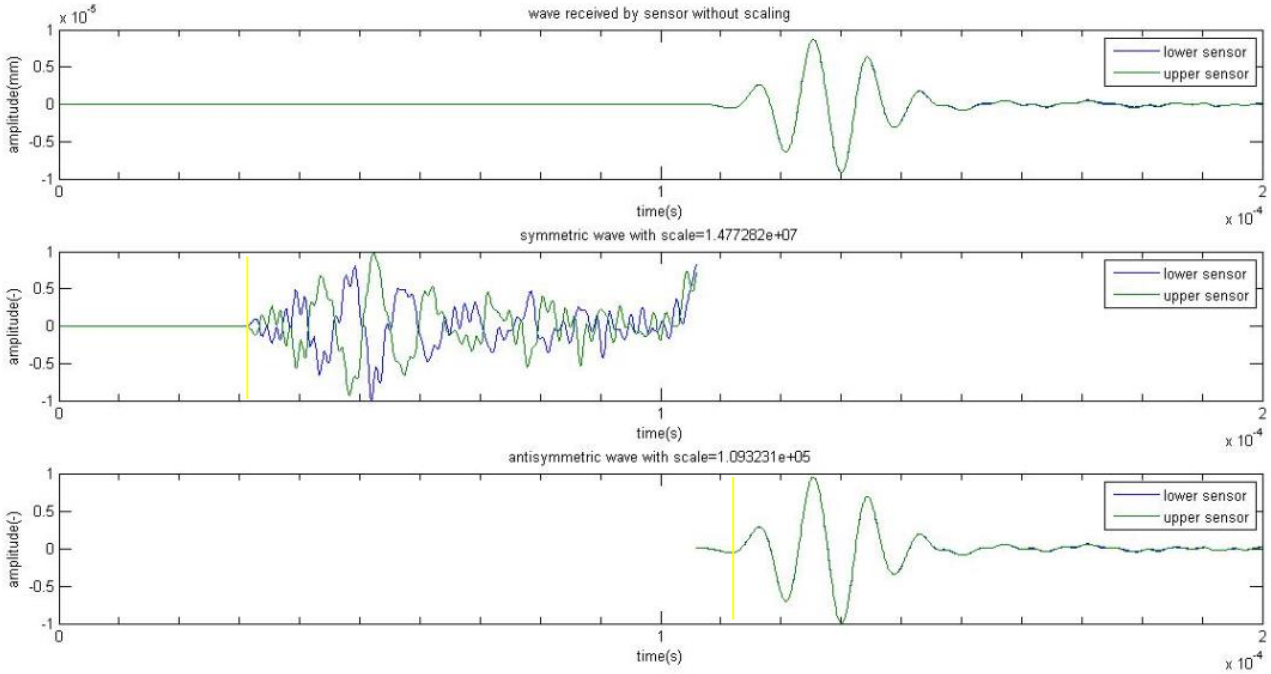

Figure 31 wave propagation in composite panel [-45°/0°/45°/45°/0°/ -45°/-45°/0°/45°]s with *crack angle of 0^0 to propagating UGW*

Configuration 4: panel with a crack with angle of 45^0 to propagating UGW

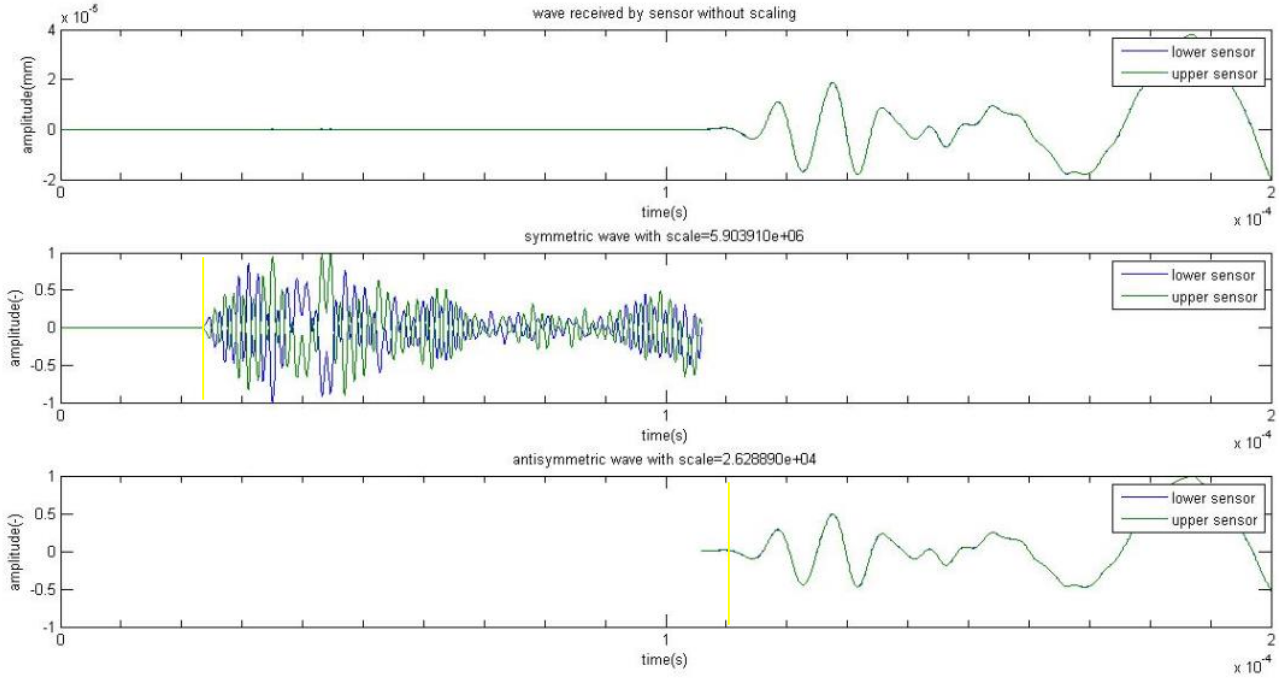

Figure 32 wave propagation in composite panel [0]12 with crack angle of 45 ^{0} to propagating UGW

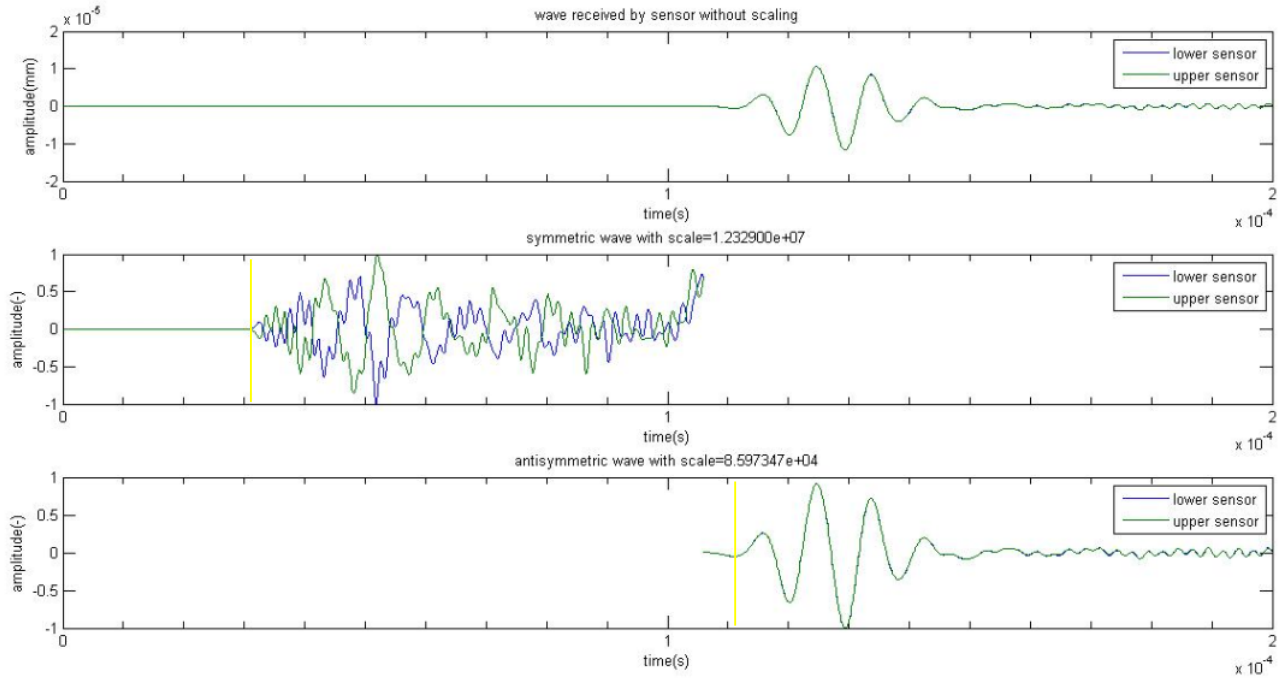

Figure 33 wave propagation in composite panel [-45°/0°/45°/45°/0°/ -45°/-45°/0°/45°]s with *crack angle of 45^0 to propagating UGW*

4.1.2 MSC.Patran/MSC.Nastran Explicit Nonlinear (SOL 700) approach

The panel, actuator, and sensors are modeled in MSC.Patran. The execution parameters are for MSC.Nastran Explicit Nonlinear (SOL 700) approach the same like for MSC.Dytran approach. In this approach data for analyzation are received from four middle nodes of actuator's and sensor's lower and upper surfaces as shown in Figure 34. These data are displacement-time data, so integration is not needed in this case.

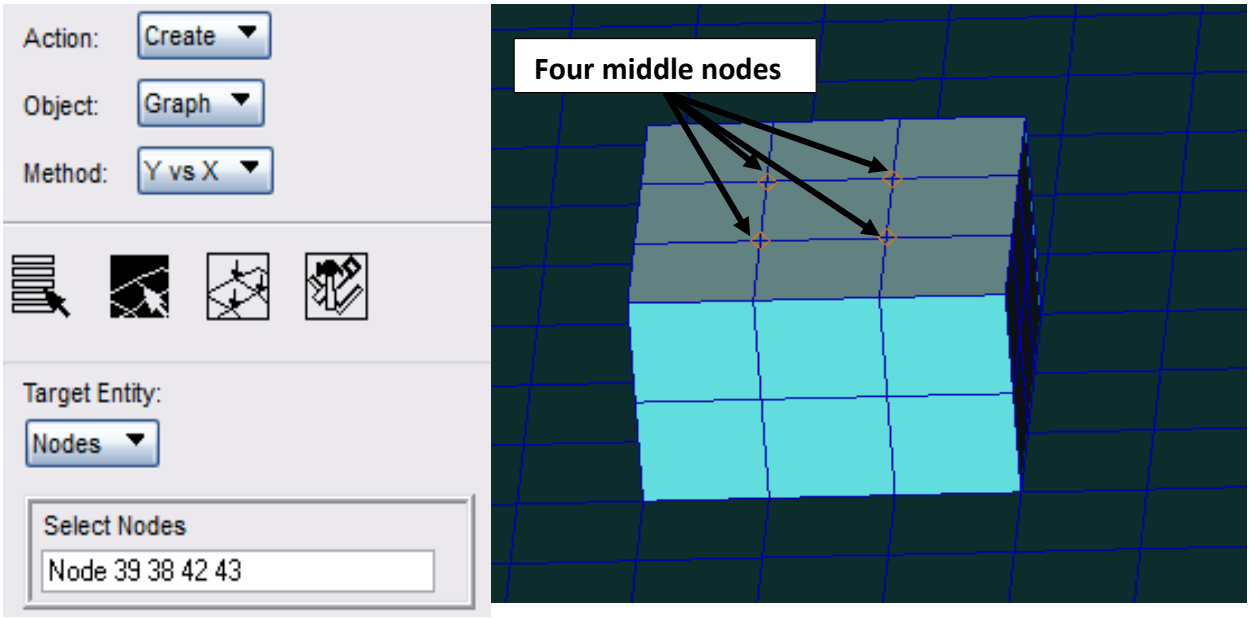

Figure 34 nodes used for analyzation of computed displacement-time data

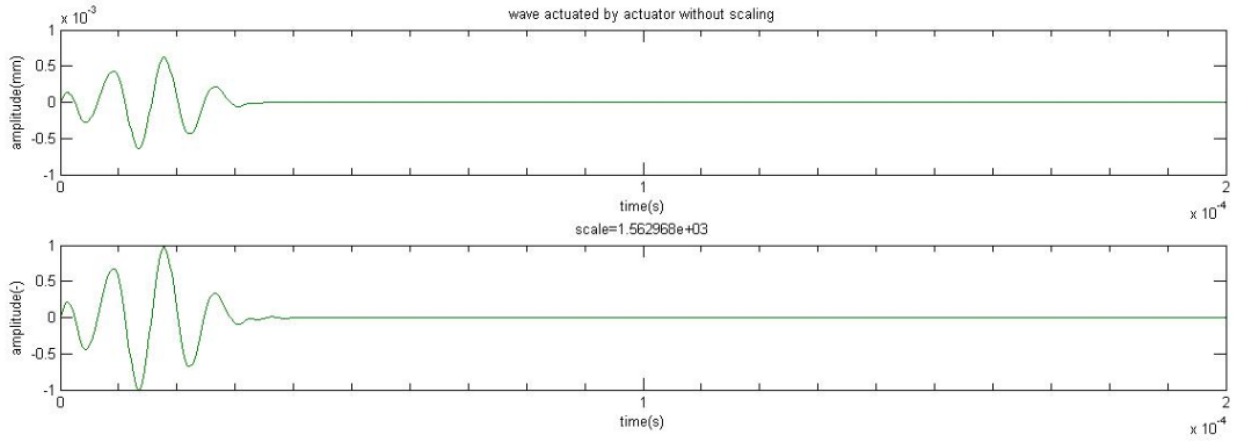

Figure 35 excitation amplitude of wave from actuator

In Figure 36 and Figure 37 bellow, comparison of wave propagation in the panel with composite structure [0]12 shown. In these two figures, interaction of waves and cracks in time is possible to observe. The highest interference is observed in configuration with cracks with angles 90^0 and 45^0. Crack with 0^0 has the lowest interference with the waves.

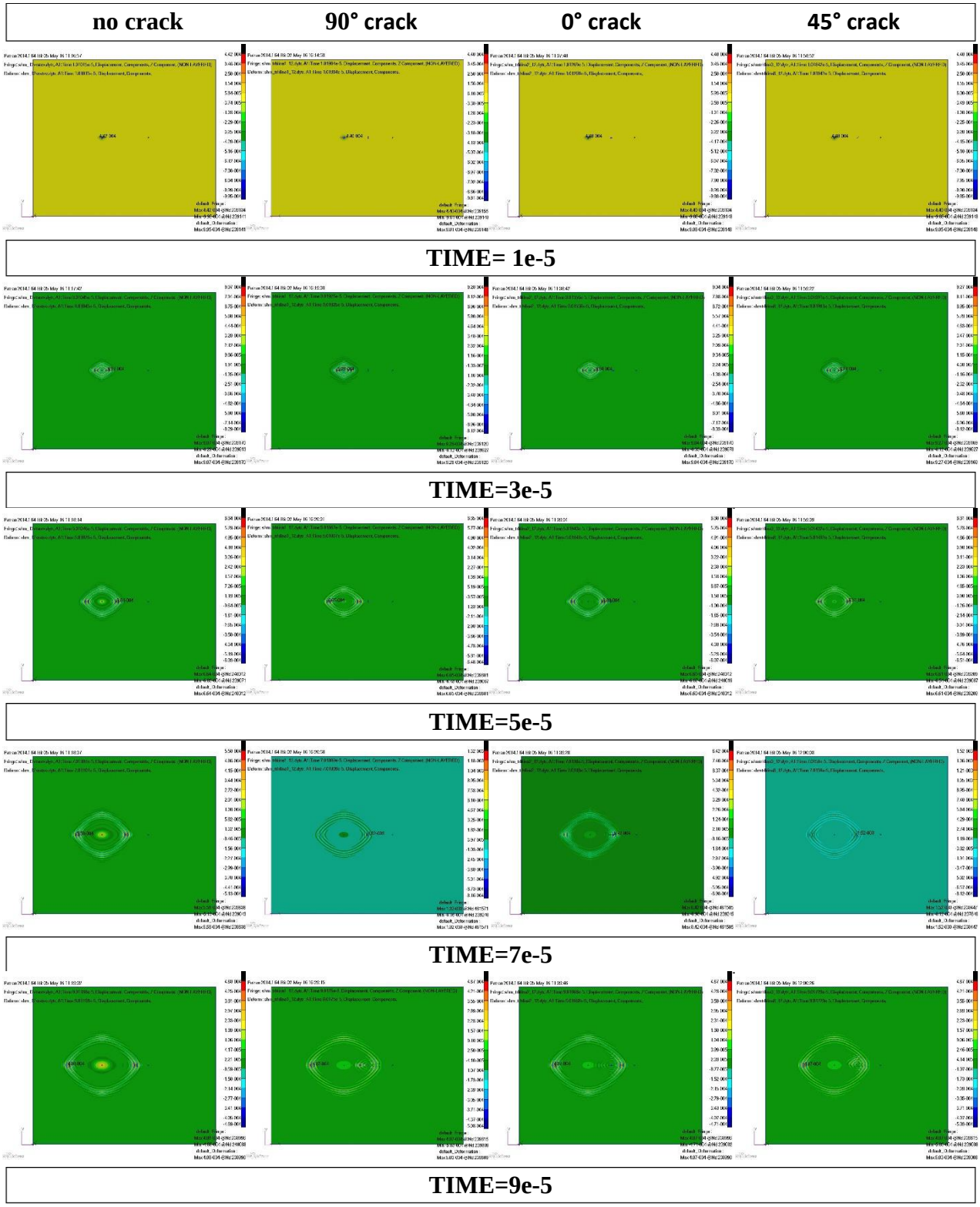

Figure 36 comparison of wave propagation in Laminate [0]12 with different cracks between piezoelectric transductors (post processor MSC.Nastran)

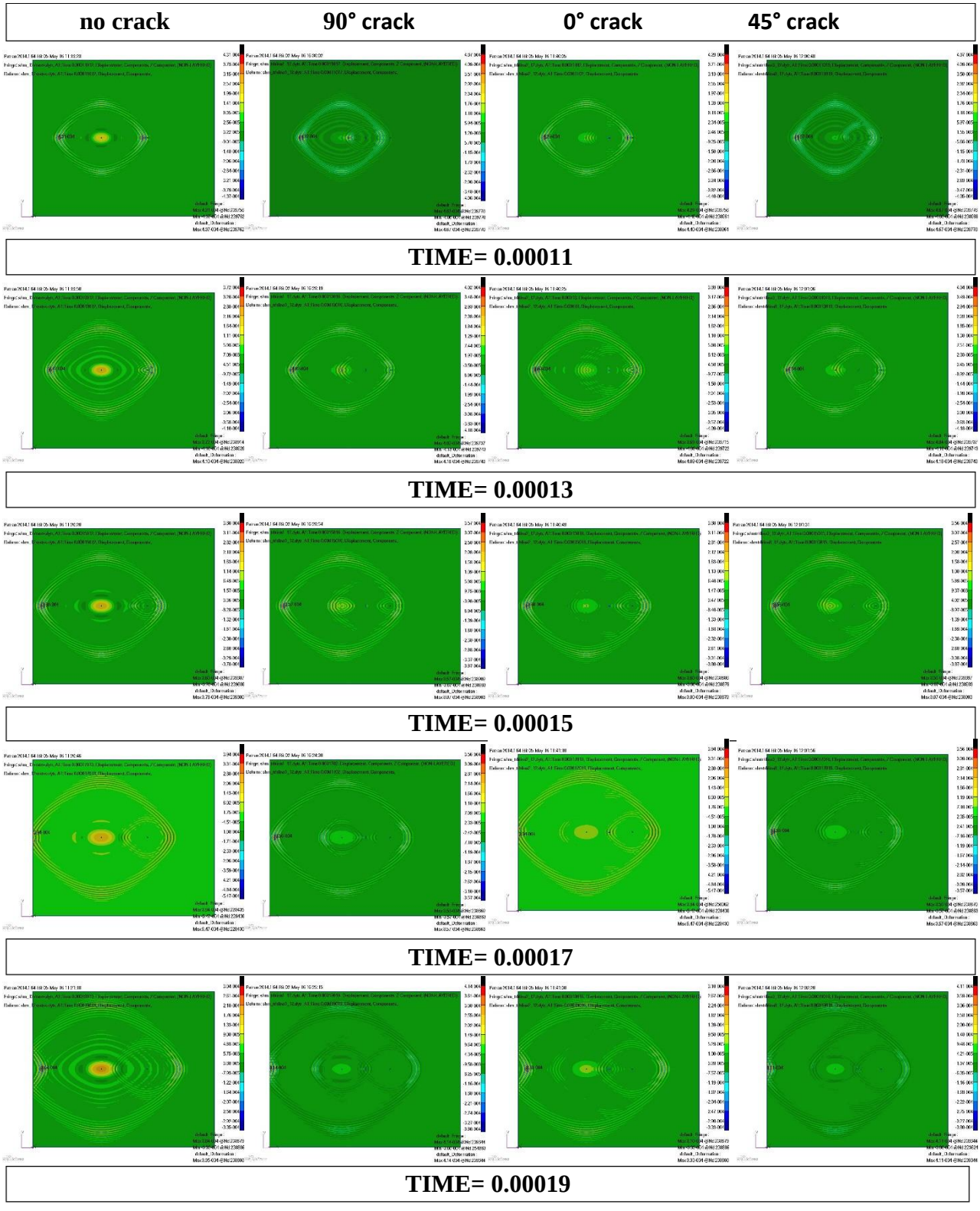

Figure 37 comparison of wave propagation in Laminate [0]12 with different cracks between piezoelectric transductors (post processor MSC.Nastran)

Configuration 1: panel without crack

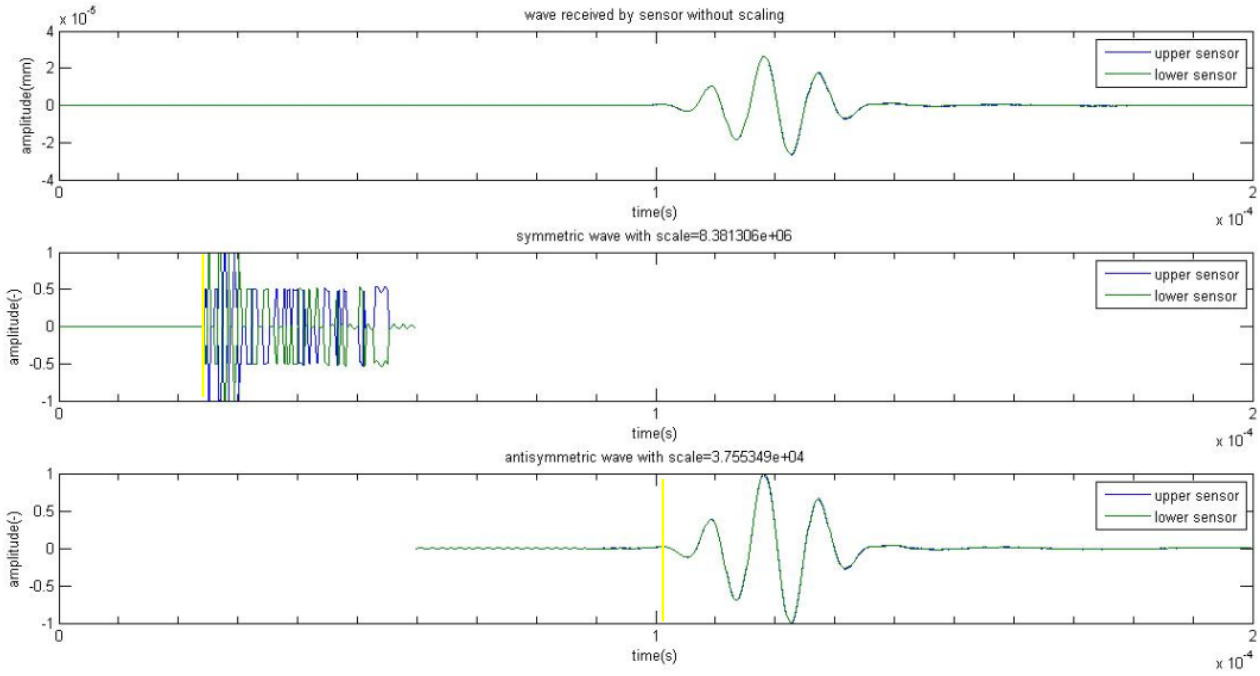

Figure 38 wave propagation in composite panel [0]12 without crack

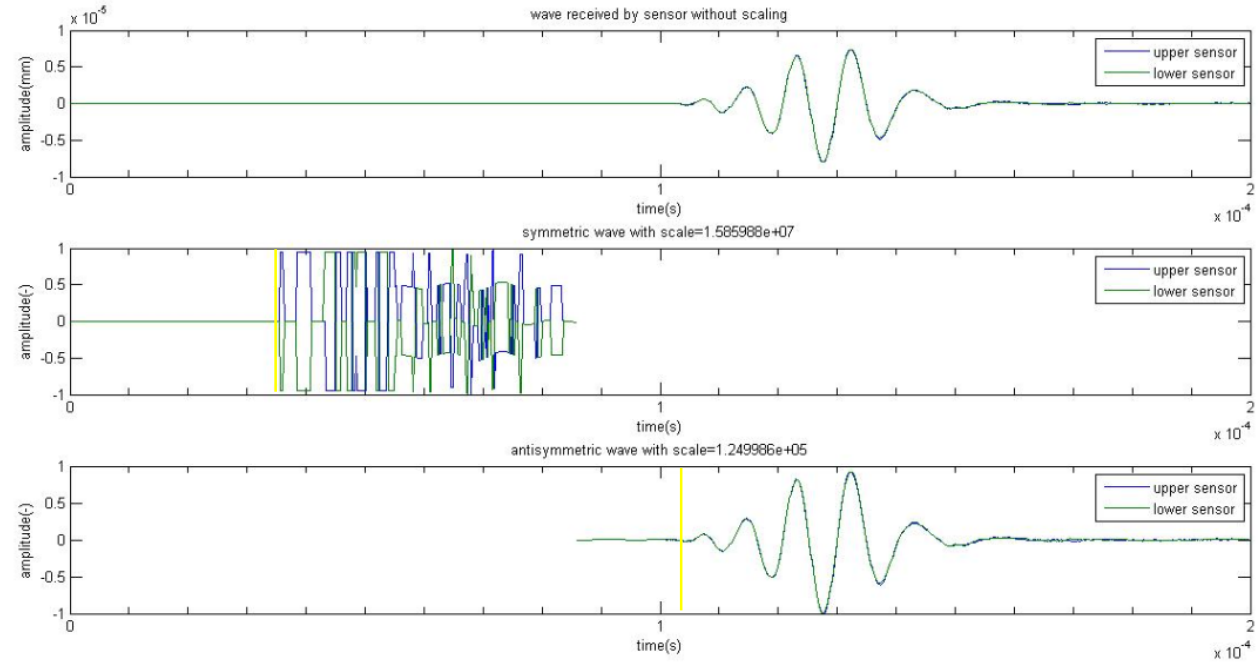

Figure 39 wave propagation in composite panel [-45°/0°/45°/45°/0°/ -45°/-45°/0°/45°]s without crack

Configuration 2: panel with a crack with angle of 90^0 to propagating UGW

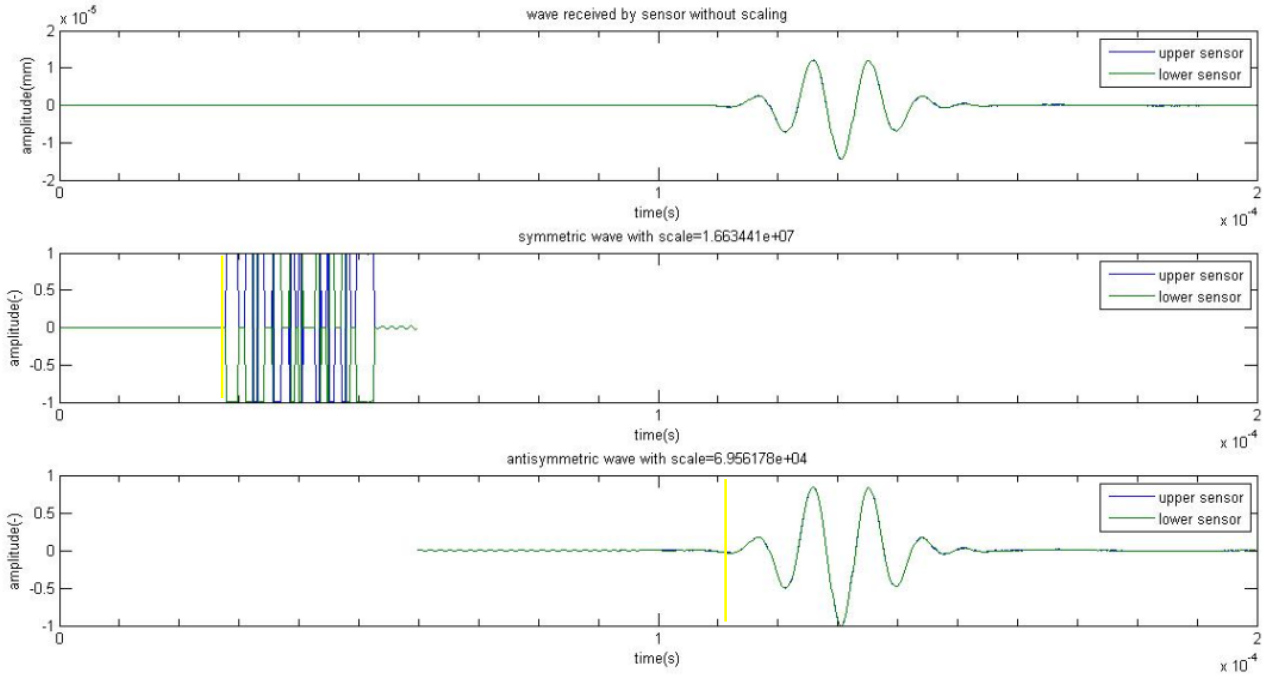

Figure 40 wave propagation in composite panel [0]12 with crack angle of 90^0 to propagating UGW

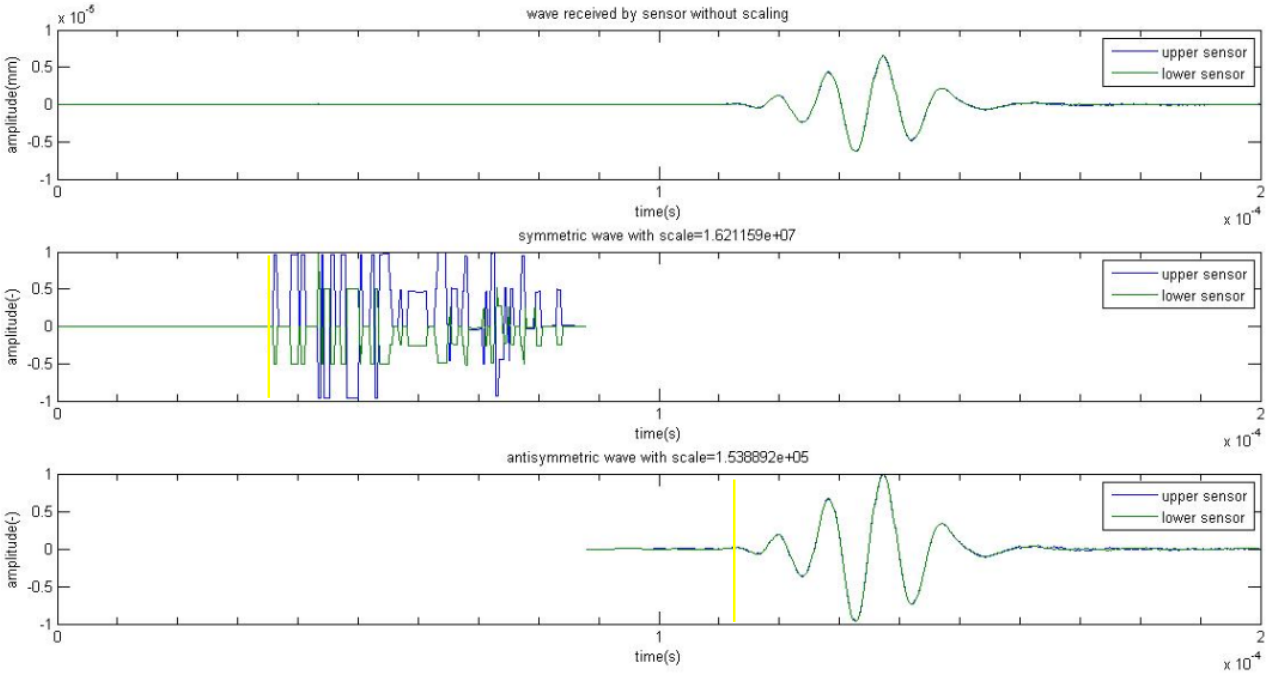

Figure 41 wave propagation in composite panel [-45°/0°/45°/45°/0°/ -45°/-45°/0°/45°]s with *crack angle of 90^0 to propagating UGW*

Configuration 3: panel with a crack with angle of 0^0 to propagating UGW

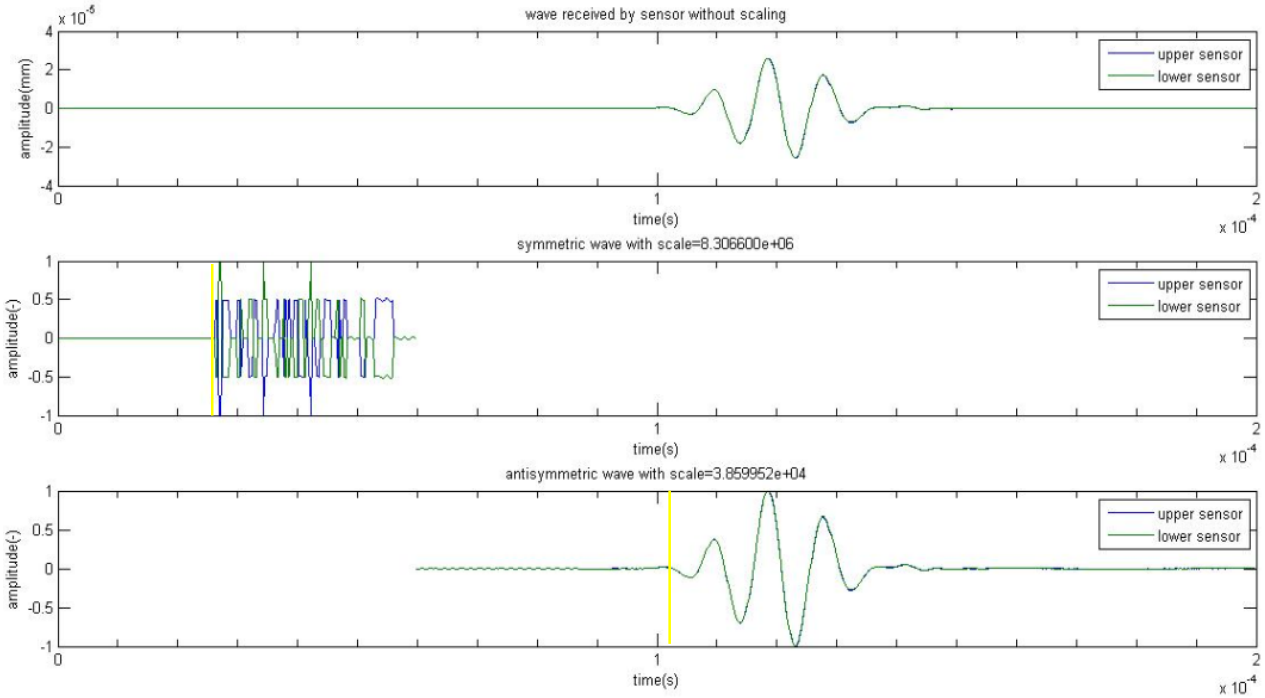

Figure 42 wave propagation in composite panel [0]12 with crack angle of 0^0 to propagating UGW

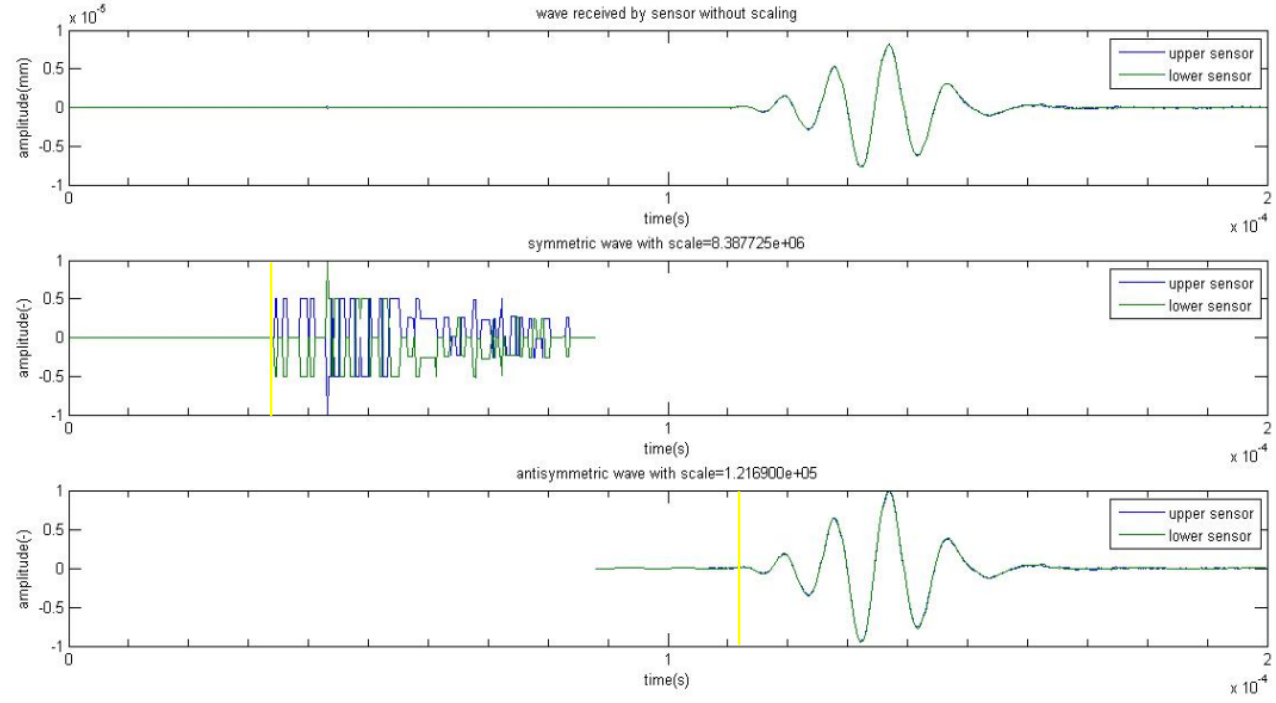

Figure 43 wave propagation in composite panel [-45°/0°/45°/45°/0°/ -45°/-45°/0°/45°]s with *crack angle of 0^0 to propagating UGW*

Configuration 4: panel with a crack with angle of 45^0 to propagating UGW

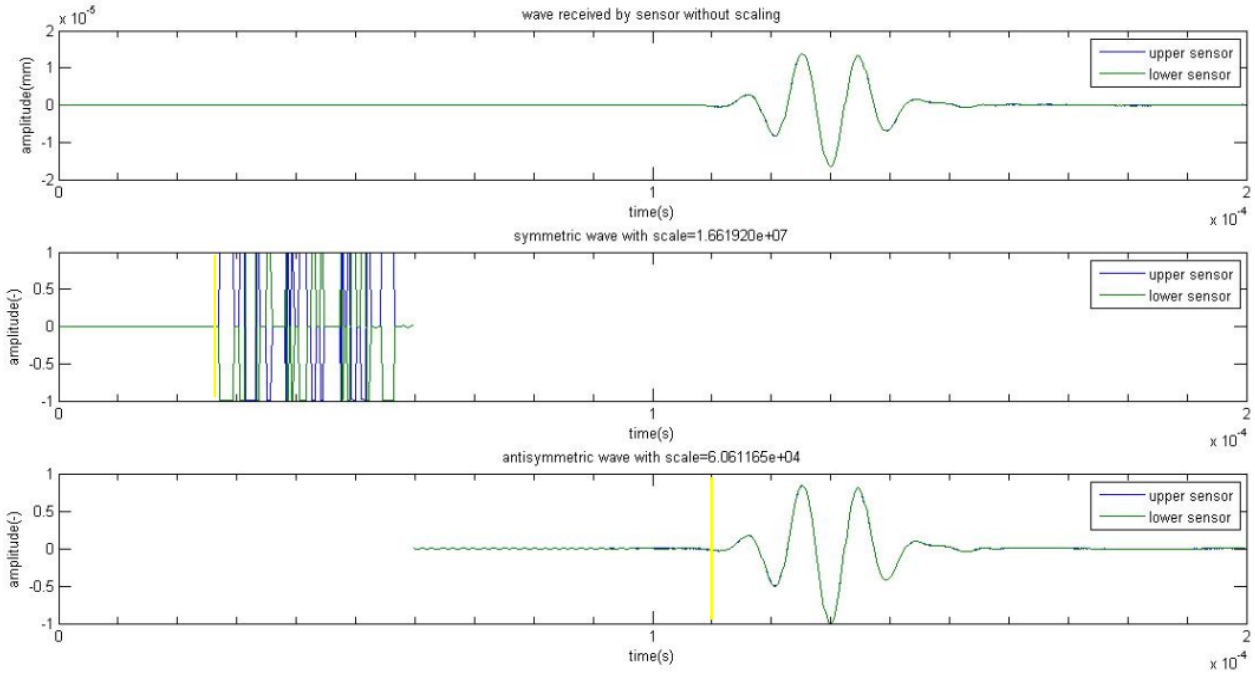

Figure 44 wave propagation in composite panel [0]12 with crack angle of 45 ^{0} to propagating UGW

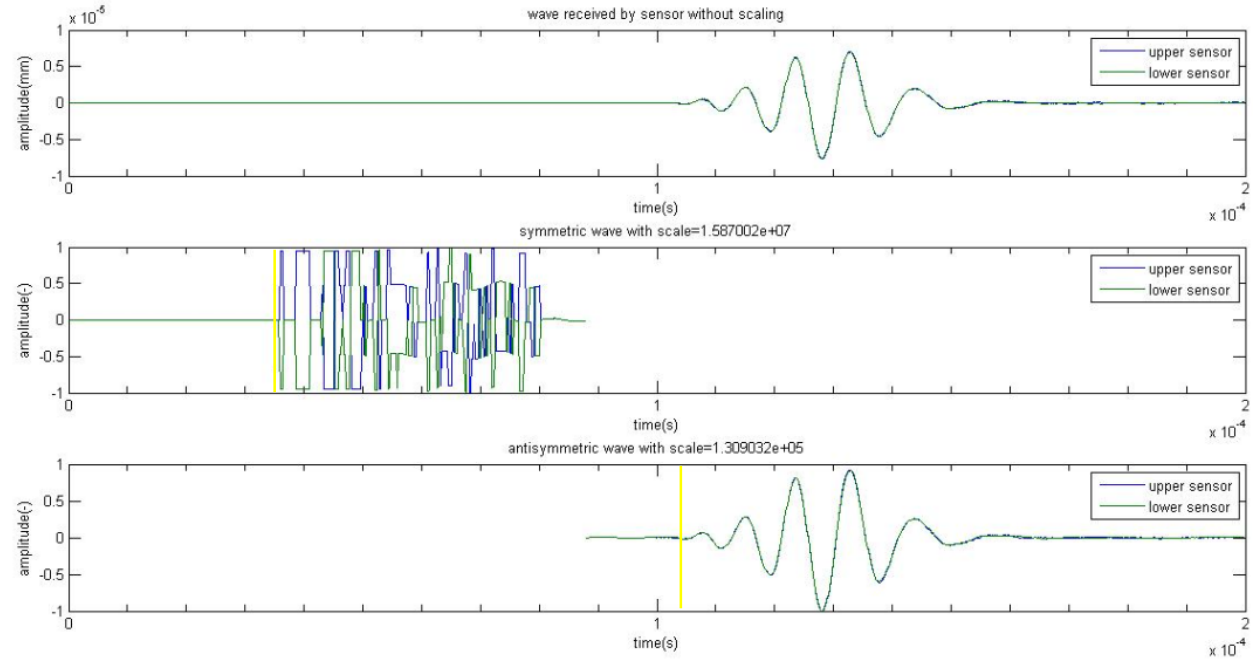

Figure 45 wave propagation in composite panel [-45°/0°/45°/45°/0°/ -45°/-45°/0°/45°]s with crack angle of 45^0 to propagating UGW

4.1.3 Analyzation of FEM results

Velocities of the waves are analyzed by the time of arrival of the wave to the sensor which is in the graphs above highlighted by the yellow line, and it is divided by the length between actuator and sensor.

$$v = \frac{l}{t} \tag{11}$$

- Where *l* = 200 mm and *t* is time of arrival of the wave to sensor

4.1.3.1 MSC.Dytran post processor

panel [0]12	Symmetric wave time of arrival [s]	Antisymmetric wave time of arrival [s]
without crack	2,26E-05	1,11E-04
90^0 crack	2,28E-05	1,12E-04
0^0 crack	2,26E-05	1,11E-04
45^0 crack	2,27E-05	1,11E-04

Table 4 symmetric and antisymmetric wave time of arrival to sensor, post processor MSC.Dytran

panel [0]12	Symmetric wave velocity [m/s]	Antisymmetric wave velocity [m/s]
without crack	8849,558	1801,802
90^0 crack	8771,93	1785,714
0^0 crack	8849,558	1801,802
45^0 crack	8810,573	1801,802

Table 5 symmetric and antisymmetric wave velocity, post processor MSC.Dytran

panel [45°/0°/45°/45°/ 0°/-45°/-45°/0°/45°]s	Symmetric wave time of arrival [s]	Antisymmetric wave time of arrival [s]
without crack	3,02E-05	1,12E-04
90^0 crack	3,03E-05	1,12E-04
0^0 crack	3,02E-05	1,12E-04
45^0 crack	3,02E-05	1,12E-04

Table 6 symmetric and antisymmetric wave time of arrival to sensor, post processor MSC.Dytran

panel [45°/0°/45°/45°/ 0°/-45°/-45°/0°/45°]s	Symmetric wave velocity [m/s]	Antisymmetric wave velocity [m/s]
without crack	6622,517	1785,714
90^0 crack	6600,66	1785,714
0^0 crack	6622,517	1785,714
45^0 crack	6622,517	1785,714

Table 7 symmetric and antisymmetric wave velocity, post processor MSC.Dytran

In the tables 4-7 with the results from MSC.Dytran, there is possible to see that waves are propagating faster in the panel [0]12. It is caused by different angles of used fibers in the composite structure. In the panel [0]12, fibers have 0^0 angle with X-axis and in this direction, waves are propagating faster than in other directions. In the panel [45°/0°/45°/45°/ 0°/-45°/-45°/0°/45°]s waves are propagating with the same velocity in each direction. Propagation of the waves in panel [0]12 and [45°/0°/45°/45°/ 0°/-45°/-45°/0°/45°]s is shown in Figure 46 and Figure 47

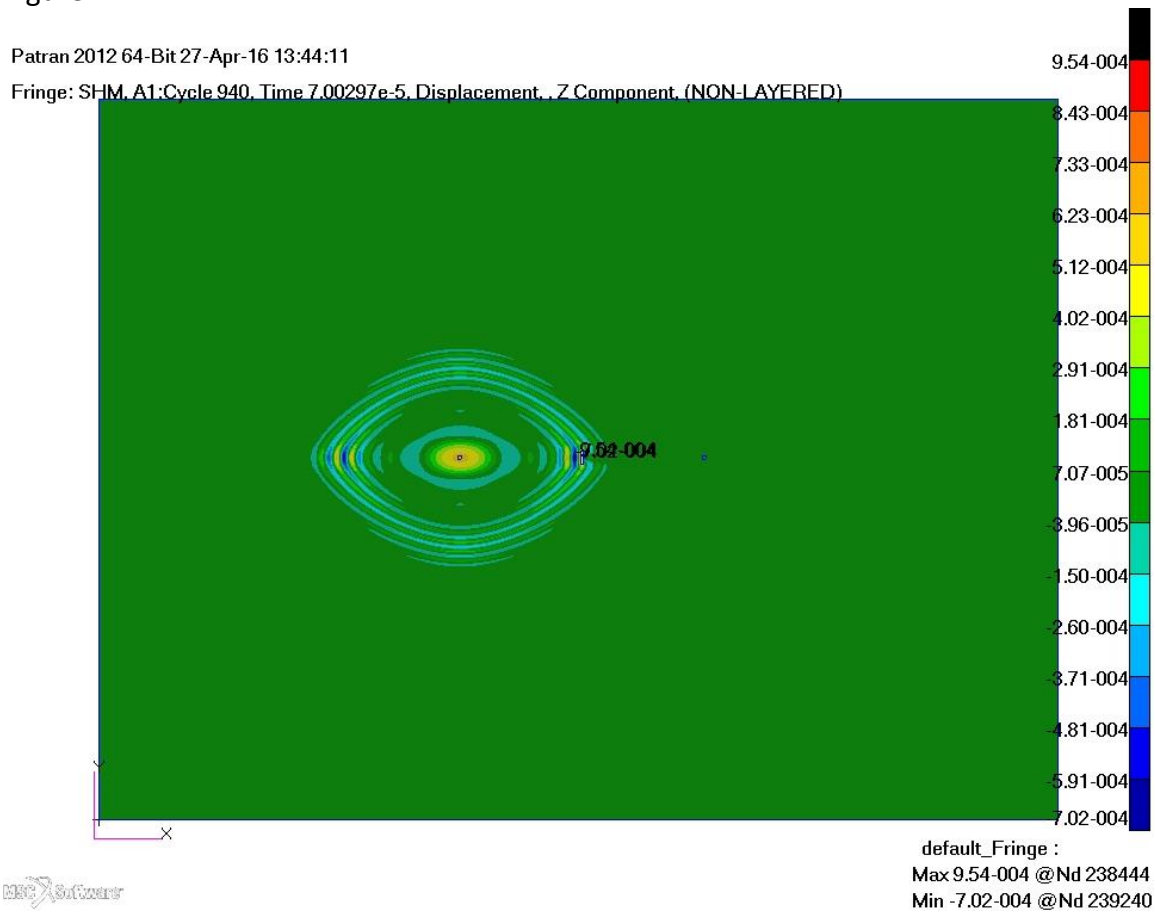

Figure 46 propagation of wawes in the panel [0]12

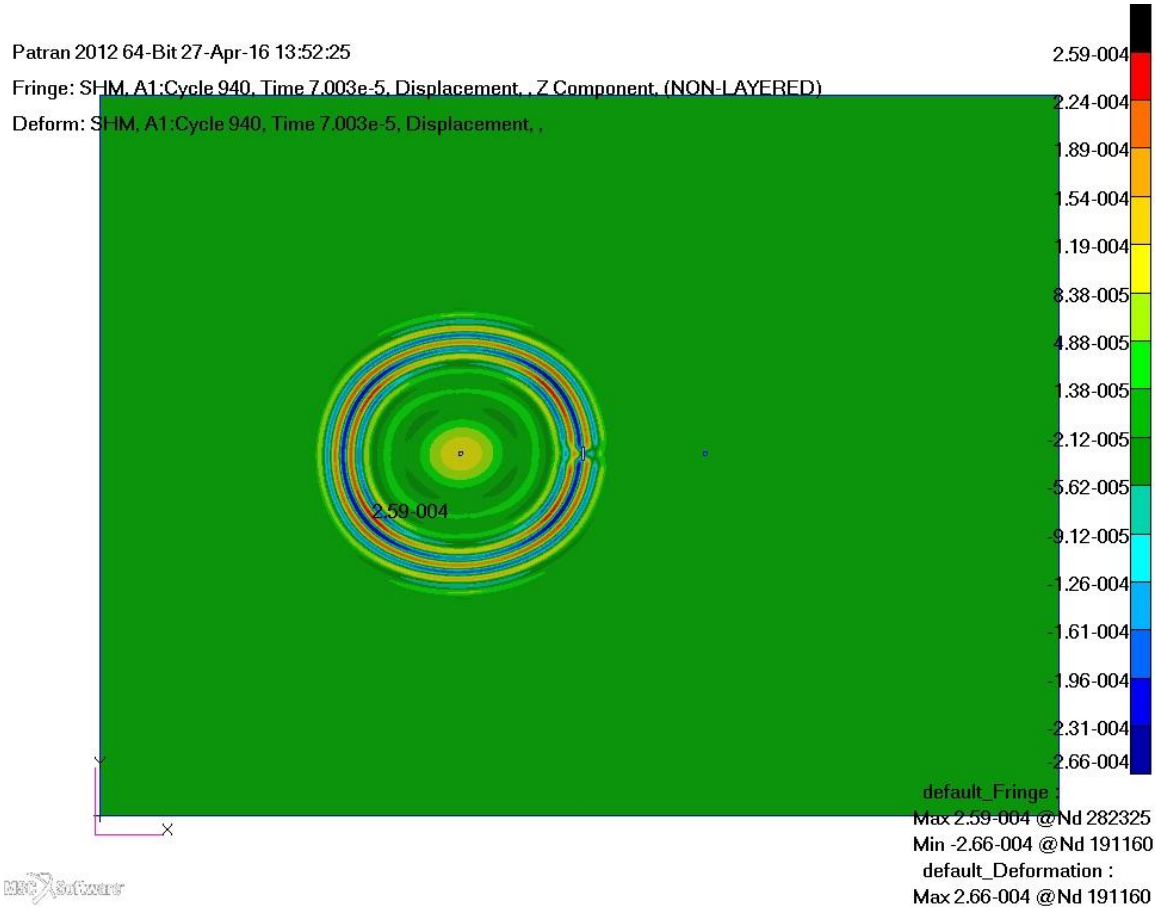

Figure 47 propagation of wawes in the panel [45°/0°/45°/45°/ 0°/-45°/-45°/0°/45°]s panel

In simulations, It is demonstrated that the crack and its angle to the propagating wave affects the velocity of the symmetric wave. The biggest difference is measured between the wave propagating in the panel without crack and the wave propagating in the panel with the crack with 90^0 angle. It is caused by the highest interference of the wave caused by the crack. However the difference of time of arrivals are very small, and there could be errors done by reading of the data. For the antisymmetric wave, the resolution of measured data is too small to find any difference. A higher difference in data is measured for the panel [0]12. Panel [45°/0°/45°/45°/ 0°/-45°/-45°/0°/45°]s is harder to be analyzed because of very small differences in the time of arrival. Velocities of symmetric and antisymmetric waves in this simulation correspond with their theoretical velocities as shown in Figure 11 Wave speed dependency of Lamb wave modes on frequencyFigure 11

panel [0]12	Symmetric wave displacement scale [-]	Antisymmetric wave displacement scale [-]
without crack	7,275176E+06	5,193209E+04
90^0 crack	1,086622E+07	9,107658E+04
0^0 crack	1,458182E+07	1,167577E+05
45^0 crack	5,903910E+06	2,628890E+04

Table 8 symmetric and antisymmetric wave displacement scale, post processor MSC.Dytran

panel [45°/0°/45°/ 45°/ 0°/-45°/-45°/0°/45°]s	Symmetric wave displacement scale [-]	Antisymmetric wave displacement scale [-]
without crack	1,263500E+07	8,236544E+04
90^0 crack	1,377472E+07	8,862996E+04
0^0 crack	1,477282E+07	1,932310E+05
45^0 crack	1,232900E+07	8,597347E+04

Table 9 symmetric and antisymmetric wave displacement scale, post processor MSC.Dytran

In Table 8 and Table 9, the results of wave displacement scales are shown. The higher the scale, the lower the amplitude is. These tables prove that if there is a crack in the panel, the amplitude of the wave is lower. In the results for panel [0]12 with 45^0 crack the results shows scale which is lower than in the panel without a crack. This error probably appeared because of disturbances after the antisymmetric wave passed the sensor as shown in the Figure 32.

4.1.3.2 MSC.Nastran Explicit Nonlinear (SOL700) post processor

panel [0]12	Symmetric wave time of arrival [s]	Antisymmetric wave time of arrival [s]
without crack	2,43E-05	1,05E-04
90^0 crack	2,77E-05	1,12E-04
0^0 crack	2,43E-05	1,05E-04
45^0 crack	2,69E-05	1,12E-04

Table 10 symmetric and antisymmetric wave time of arrival to sensor, post processor MSC.Nastran (SOL700)

panel [0]12	Symmetric wave velocity [m/s]	Antisymmetric wave velocity [m/s]
without crack	8230,453	1904,762
90^0 crack	7220,217	1785,714
0^0 crack	8230,453	1904,762
45^0 crack	7434,944	1785,714

Table 11 symmetric and antisymmetric wave velocity, post processor MSC.Nastran (SOL700)

panel [45°/0°/45°/45°/0°/-45°/-45°/0°/45°]s	Symmetric wave time of arrival [s]	Antisymmetric wave time of arrival [s]
without crack	3,55E-05	1,02E-04
90^0 crack	3,59E-05	1,14E-04
0^0 crack	3,43E-05	1,02E-04
45^0 crack	3,58E-05	1,12E-04

Table 12symmetric and antisymmetric wave time of arrival to sensor, post processor MSC.Nastran (SOL700)

panel [45°/0°/45°/45°/0°/-45°/-45°/0°/45°]s	Symmetric wave velocity [m/s]	Antisymmetric wave velocity [m/s]
without crack	5633,803	1904,762
90^0 crack	5571,031	1754,386
0^0 crack	5830,904	1904,386
45^0 crack	5586,592	1904,762

Table 13 symmetric and antisymmetric wave velocity, post processor MSC.Nastran (SOL700)

In tables 10-13 with the results from MSC.Nastran Explicit Nonlinear (SOL700) symmetric and antisymmetric wave velocity for different configurations are compared. Results again prove that cracks affecting the velocity of the waves. In configurations where the crack in the panel is modeled, lower UGW propagation velocity is measured. This is again proved only for the symmetric waves. For the antisymmetric waves, the results are again too similar to find any difference because of the hard estimation of more accurate wave time of arrival to the sensor. Velocities of symmetric and antisymmetric waves in this simulation correspond with their theoretical velocities as shown in Figure 11 Wave speed dependency of Lamb wave modes on frequencyFigure 11

panel [0]12	Symmetric wave displacement scale [-]	Antisymmetric wave displacement scale [-]
without crack	8,381306E+06	3,755349E+04
90^0 crack	1,663440E+07	6,956178E+04
0^0 crack	8,306600E+06	3,859952E+04
45^0 crack	1,661920E+07	6,061165E+04

Table 14 symmetric and antisymmetric wave displacement scale, post processor MSC.Nastran (SOL700)

panel [45°/0°/45°/45°/0°/-45°/-45°/0°/45°]s	Symmetric wave displacement scale [-]	Antisymmetric wave displacement scale [-]
without crack	1,585988E+07	1,249986E+05
90^0 crack	1,621159E+07	1,538892E+05
0^0 crack	8,387725E+06	1,216900E+05
45^0 crack	1,587002E+07	1,309032E+05

Table 15 symmetric and antisymmetric wave displacement scale, post processor MSC.Nastran (SOL700)

In Table 14 and Table 15 with results using MSC.Nastran(SOL700) postprocessor, there is a comparison of used scales for normalization of the amplitude of the waves. As shown in these tables, scales of configuration with panels with cracks are higher than in configuration without a crack. This is proved for both symmetric and antisymmetric wave. Only in the case, where symmetric wave is propagating in panel with 0^0 crack, higher amplitude is measured. It is caused by one peak in the symmetric wave which is twice bigger than average amplitude as shown in Figure 42 and Figure 43.

In the Figure 48 there is a comparison of two simulations with highest differences in results. It is a configuration without the crack and with the crack with 90^0 angle. In the top and bottom plot in Figure 48 the difference in the time of arrival and the amplitude of antisymmetric wave is clear. In the middle plot in Figure 48, where symmetric waves are scaled it is clear that wave in the panel with the crack with 90^0 angle is propagating slower as is already shown in *Table 10* and Table 11. It is also obvious that the higher amplitude of symmetric wave is different only in first four periods and then the amplitude in both cases is the same. This is found also in other cases, that there are only few peaks, which makes the scale larger during the propagation but most periods of symmetric waves have the same amplitude.

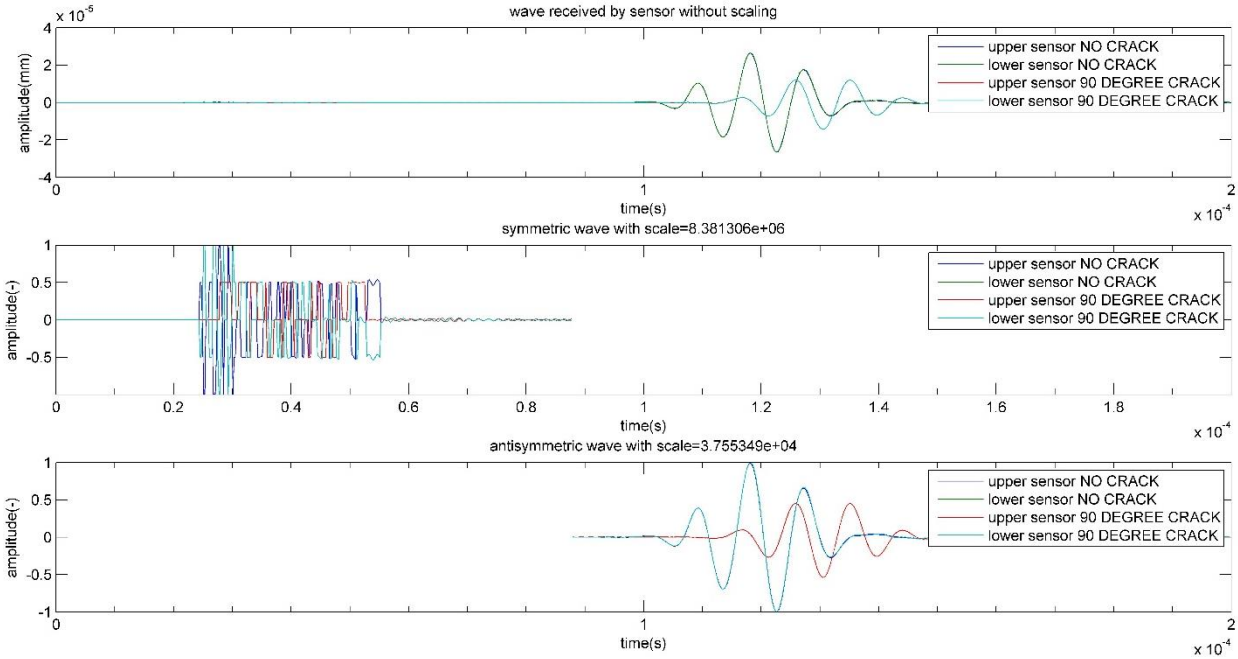

Figure 48 comparison of wave propagating in the panel without crack and in the panel with 90^0crack*, post processor MSC.Nastran (SOL700)*

5. Conclusion

In this thesis structural health monitoring techniques and their usage for aircraft maintenance is described. The main goal of this thesis, simulation of UGW propagation using preprocessor MSC.Patran and two post processors for comparison of results is done. The first post processor is MSC.Dytran and the second post processor is MSC.Nastran Explicit Nonlinear (SOL700). Simulation is done for the pitch-catch method which consists of an actuator which exciting the signal and a sensor which sensing the signal. For the purpose of investigating UGW propagation and its characteristics during the propagation, panels with different materials and different cracks are used.

The results from these two post processors with different approaches shows that both post processors can be used for simulation of UGW propagation. The difference in results of both post processors are between 4%-7% and in some cases, the results are identical. Highest differences are in the velocities of symmetric waves, where more accurate reading of data due to the character of the waves is done. The difference in results between these two post processors for symmetric waves is about 7%. Velocities of symmetric waves are smaller in the results, where MSC.Nastran(SOL700) approach is used.

The difference in results is also in the propagation of symmetric waves. In the results solved by MSC.Dytran, symmetric waves are passing through the sensor much longer time and in the end continuously changing into antisymmetric wave as shown in Figure 26. Results from MSC.Patran(SOL700) shows symmetric wave, then “space” with zero amplitude and after it antisymmetric wave. This is more accurate result of the simulation of the wave, and it is shown in Figure 38.

In both post processors, it was proved that cracks are changing the amplitude of symmetrical and antisymmetrical waves. In the panels with modeled crack, amplitudes of the antisymmetric waves are smaller in comparison with the panel without cracks. For the symmetric waves, only few periods with highest peaks affecting the scale but rest of the wave’s amplitude is the same for all cases.

Both post processors verified that velocity of the waves is decreased by the crack between actuator and sensor. The lowest speed is measured in configuration with 90^0 degree crack. From both used post processors only velocity for symmetric waves is measured accurately. For the antisymmetric wave, it is hard to estimate the accurate time of arrival and in most simulated cases, the velocity is almost the same.

The approach using MSC.Dytran as a post processor takes less time, but the data are not as accurate as results from MSC.Patran(SOL700). Furthermore analyzation of data and estimating the most accurate time of arrival of the symmetric wave is in this case possible only with data from MSC.Patran(SOL700).

For the future analyses of UGW propagation with different configurations MSC.Patran(SOL700) should be considered as the main post processor. It takes longer time for calculation the data from MSC.Nastran and after it, it is also more time-consuming for the preparation of the data for calculations in Matlab. On the other hand, the final data are very precise and much easier to be analyzed.

6. References

1. *Wavelet Transform for Structural Health Monitoring: A Compendium of Uses and Features.* Taha, M. M. Reda. 2006, Structural Health Monitoring.

2. Bisht, Saurabh S. *Methods for Structural Health Monitoring and Damage Detection of Civil and Mechanical Systems.* Blacksburg, Virginia : s.n., 2005.

3. Han, SeJin. *Finite element analysis of lamb waves acting within a thin aluminum plate.* September 2007.

4. Jian Cai, Lei Qiu, Shenfang Yuan, Lihua Shi, PeiPei Liu and Dong Liang. *Structural Health Monitoring for Composite Materials.*

5. Speckmann, Holger. *Structural Health Monitoring.* Bremen, Germany : s.n., January 29, 2008.

6. *Boundless.com.* [Online] https://www.boundless.com/physics/textbooks/boundless-physics-textbook/waves-and-vibrations-15/waves-125/longitudinal-waves-439-5596/.

7. Ahmed, Mustofa Nurhussien. *A study of guided ultrasonic wave propagation characteristics in thin aluminium plate for damage detection.* Toledo, Spain : s.n., May 2014.

8. *Guided Lamb waves for identification of damage in composite structures.* Zhongqing Su, Lin Ye, Ye Lu. 2006, Journal of Sound and Vibration.

9. *Two Dimensional FEM Simulation of Ultrasonic Wave Propagation in Isotropic Solid Media using COMSOL.* Bikash Ghose, Krishman Balasubramaniam, C V Krishnamurthy, A Subhananda Rao. 2010. COMSOL Conference 2010 India .

10. MSC Software. [Online] http://www.mscsoftware.com/.

11. *MSC. Nastran 2014 Explicit Nonlinear (SOL700) User's Guide , 2014 MSC.Software Corporation. Printed in U.S.A. All Rights Reserved.*

12. Daubechies. *Ten Lectures on Wavelets.* s.l. : Soc. for Industrial and Applied Math, 1992.

13. *MSC.Dytran 2012 Reference Manual, 2012 MSC.Software Corporation. Printed in U.S.A. All Rights Reserved*

7. Appendix:

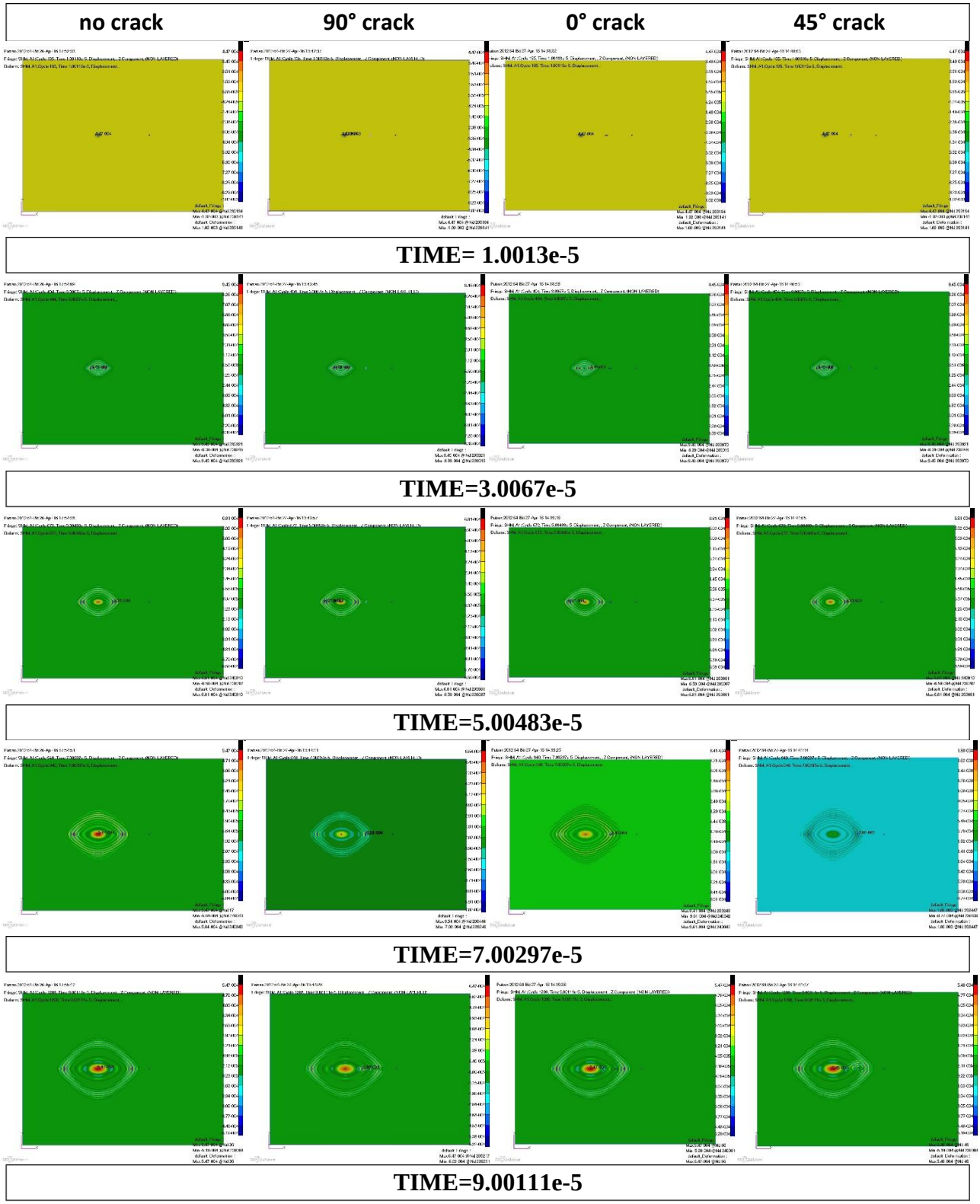

appendix 1: comparison of wave propagation in Laminate [0]12 with different cracks between piezoelectric transductors (post processor MSC.Dytran)

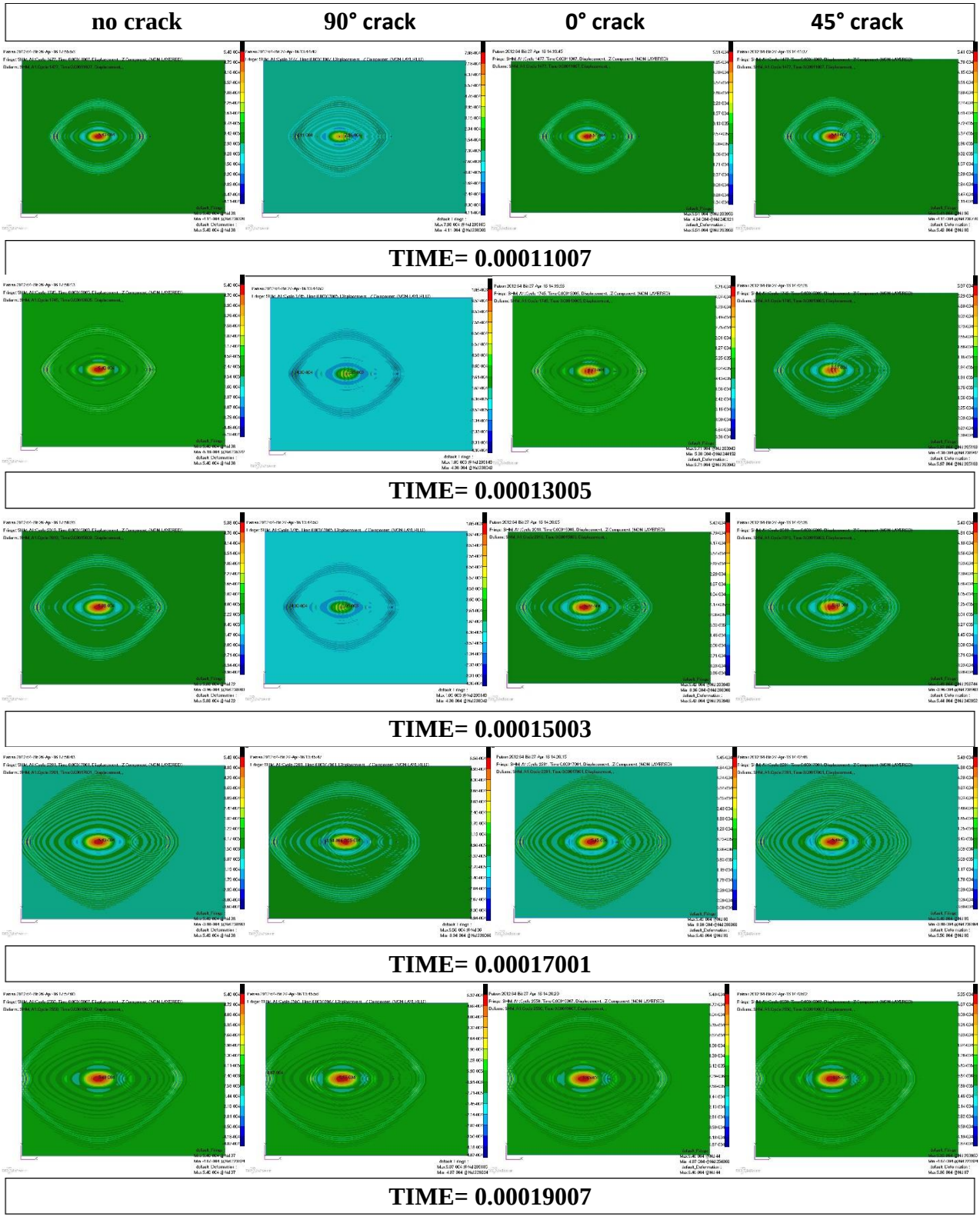

appendix 2: comparison of wave propagation in Laminate [0]12 with different cracks between piezoelectric transductors (post processor MSC.Dytran)

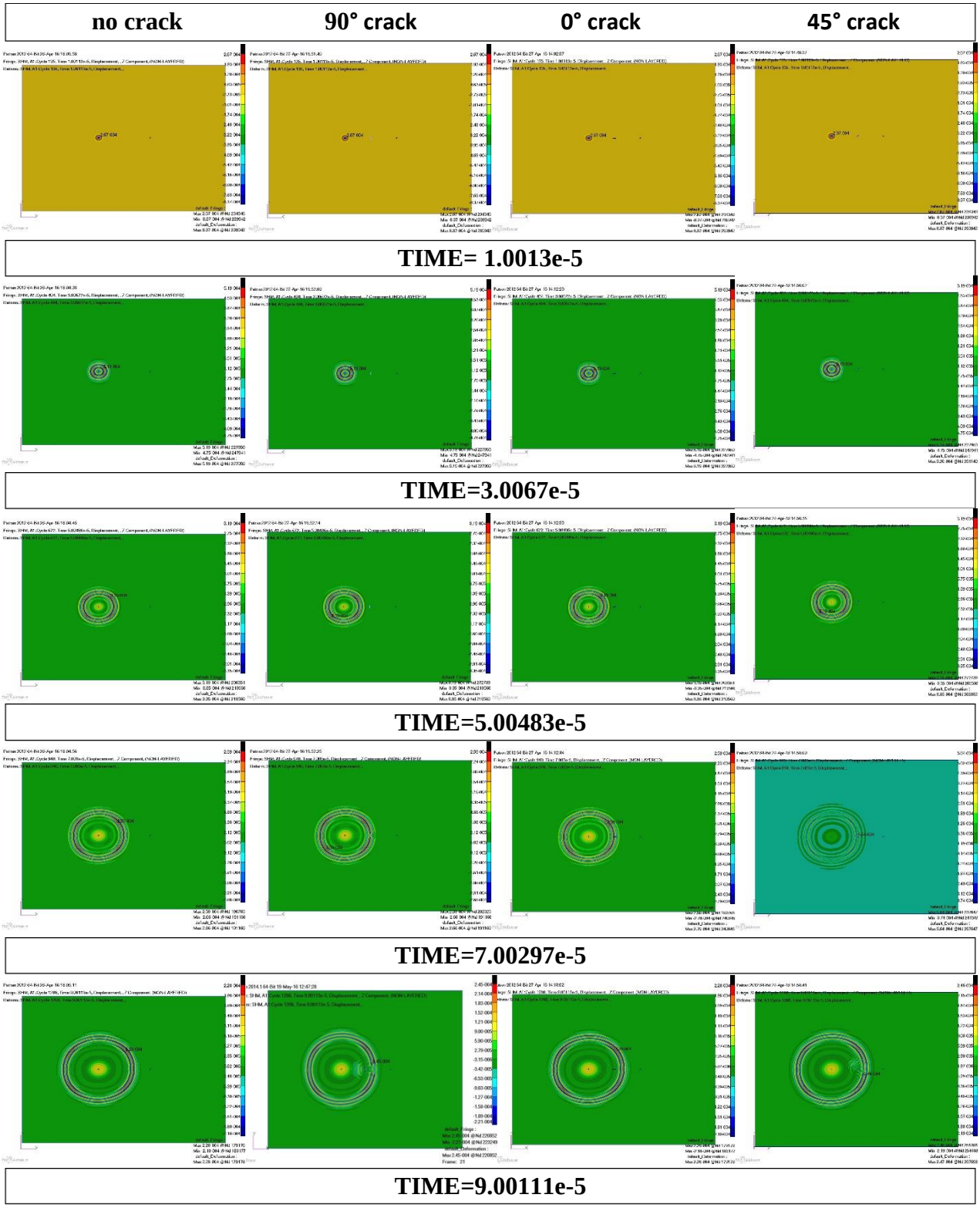

appendix 3: comparison of wave propagation in [-45°/0°/45°/45°/0°/-45°/-45°/0°/45°]s with different cracks between piezoelectric transductors (post processor MSC.Dytran)

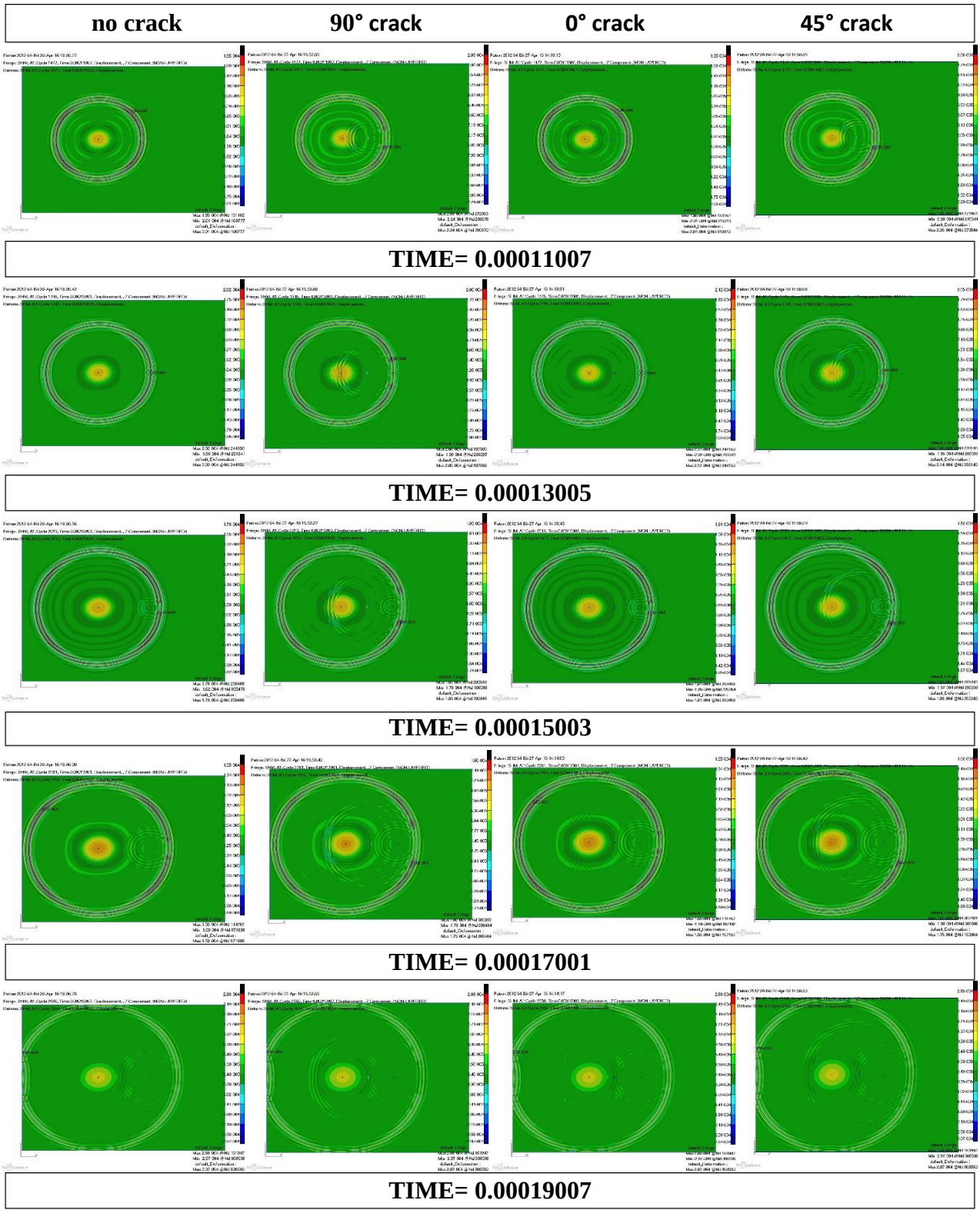

appendix 4: comparison of wave propagation in [-45°/0°/45°/45°/0°/-45°/-45°/0°/45°]s with different cracks between piezoelectric transductors (post processor MSC.Dytran)

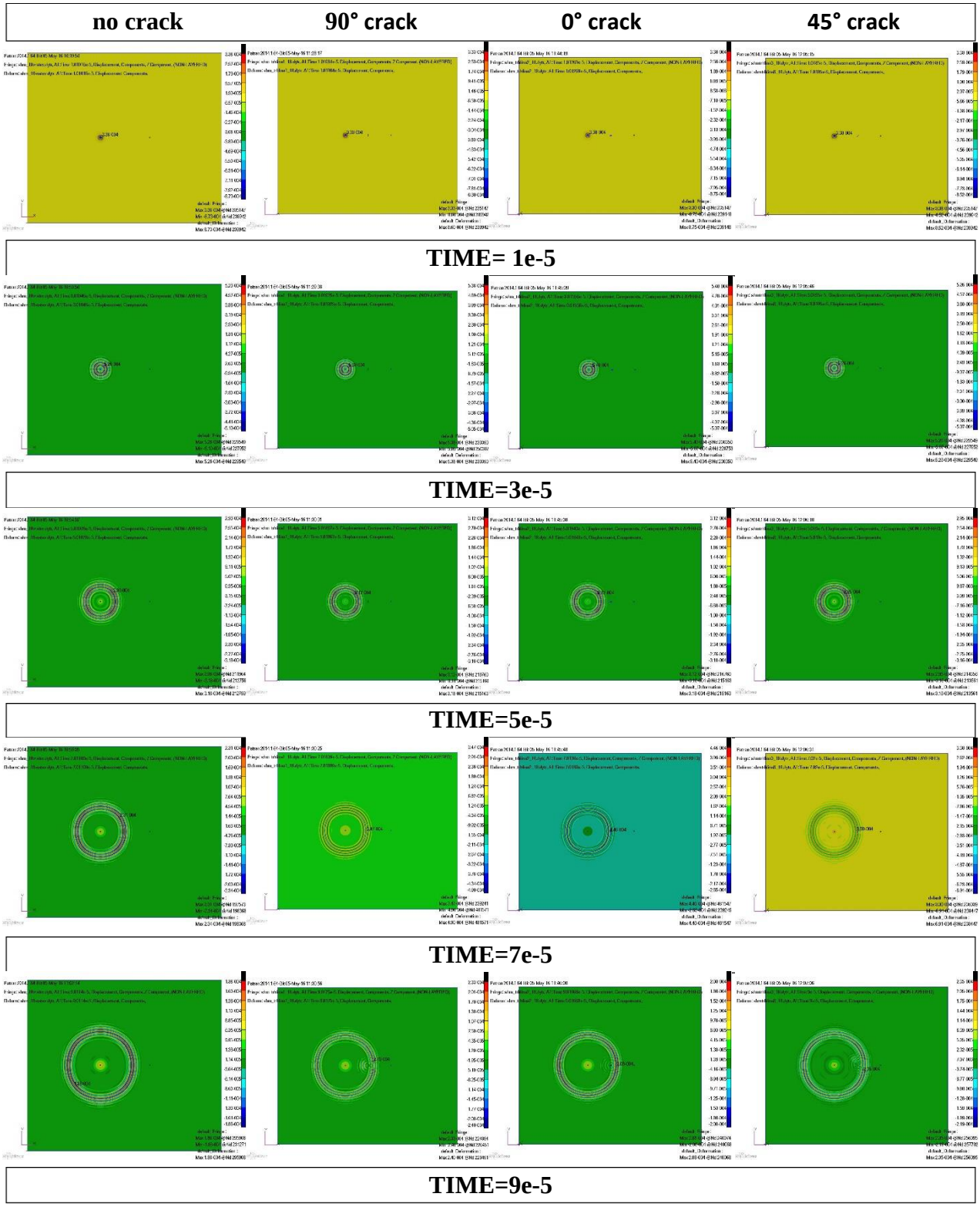

appendix 5: comparison of wave propagation in [-45°/0°/45°/45°/0°/-45°/-45°/0°/45°]s with different cracks between piezoelectric transductors (post processor MSC.Nastran)

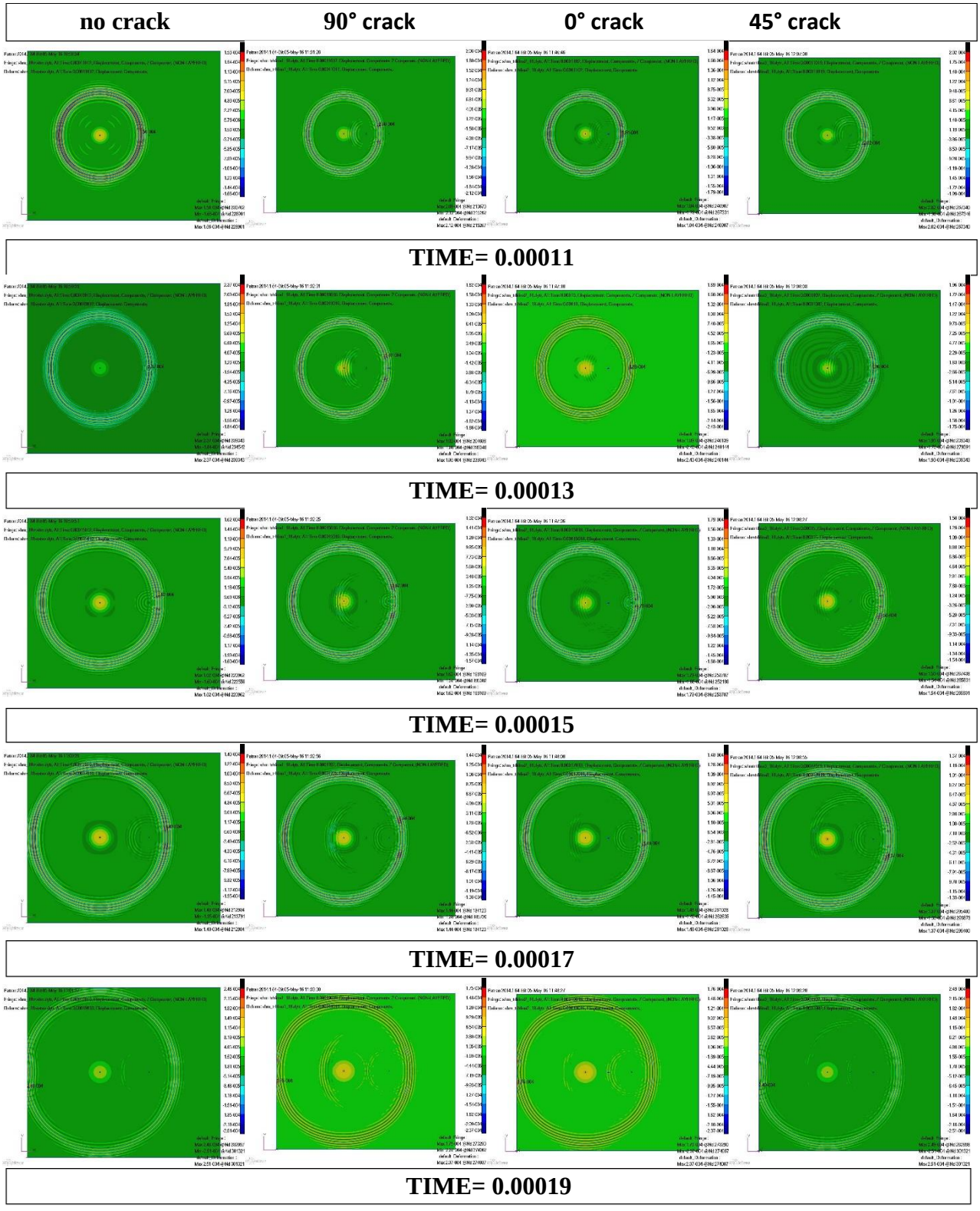

appendix 6: comparison of wave propagation in [-45°/0°/45°/45°/0°/-45°/-45°/0°/45°]s with different cracks between piezoelectric transductors (post processor MSC.Nastran)